Correcting model biases of CO in East Asia: impact on oxidant distributions during KORUS-AQ

Benjamin Gaubert[1], Louisa K. Emmons[1], Kevin Raeder[2], Simone Tilmes[1], Kazuyuki Miyazaki[3], Avelino. F. Arellano Jr[4], Nellie Elguindi[5], Claire Granier[5,6], Wenfu Tang[7], Jérôme Barré[8], Helen M. Worden[1], Rebecca R. Buchholz[1], David P. Edwards[1], Philipp Franke[9], Jeffrey L. Anderson[2], Marielle Saunois[10], Jason Schroeder[11], Jung-Hun Woo[12], Isobel J. Simpson[13], Donald R. Blake[13], Simone Meinardi[13], Paul O. Wennberg[14], John Crounse[14], Alex Teng[14], Michelle Kim[14], Russell R. Dickerson[15,16], Hao He[15,16], Xinrong Ren[15,17], Sally E. Pusede[18], Glenn S. Diskin[19]

[1]Atmospheric Chemistry Observations and Modeling, National Center for Atmospheric Research, Boulder, CO, USA.
[2]Computational and Information Systems Laboratory, National Center for Atmospheric Research, Boulder, CO, USA.
[3]Jet Propulsion Laboratory, California Institute of Technology, Pasadena, CA, USA.
[4]Dept. of Hydrology and Atmospheric Sciences, University of Arizona, Tucson, AZ, USA.
[5]Laboratoire d'Aérologie, CNRS, Université de Toulouse, France.
[6]NOAA Chemical Sciences Laboratory-CIRES/University of Colorado, Boulder, CO, USA.
[7]Advanced Study Program, National Center for Atmospheric Research, Boulder, CO, USA.
[8]European Centre for Medium-Range Weather Forecasts, Shinfield Park, Reading, RG2 9AX, UK.
[9]Forschungszentrum Jülich GmbH, Institut für Energie und Klimaforschung IEK-8, 52425 Jülich, Germany.
[10]Laboratoire des Sciences du Climat et de l'Environnement, LSCE-IPSL (CEA-CNRS-UVSQ), Université Paris-Saclay, 91191 Gif-sur-Yvette, France.
[11]California Air Resources Board, Sacramento, CA, USA.
[12]Department of Advanced Technology Fusion, Konkuk University, Seoul, South Korea.
[13]Department Chemistry, University of California, Irvine, Irvine, CA 92697, USA.
[14]California Institute of Technology, Pasadena, CA, USA.
[15]Department of Atmospheric and Oceanic Science, University of Maryland, College Park, MD, USA.
[16]Earth System Science Interdisciplinary Center, University of Maryland, College Park, MD, USA.
[17]Air Resources Laboratory, National Oceanic and Atmospheric Administration, College Park, MD, USA.
[18]Department of Environmental Sciences, University of Virginia, Charlottesville, VA, USA.
[19]NASA Langley Research Center, Hampton, VA, USA.

Correspondence to: Benjamin Gaubert (gaubert@ucar.edu)

Abstract. Global coupled chemistry-climate models underestimate carbon monoxide (CO) in the Northern Hemisphere, exhibiting a pervasive, negative bias against measurements peaking in late winter and early spring. While this bias has been commonly attributed to underestimation of direct anthropogenic and biomass burning emissions, chemical production and loss via OH reaction from emissions of anthropogenic and biogenic VOCs play an important role. Here we investigate the reasons for this underestimation using aircraft measurements taken in May and June 2016 from the Korea United States Air Quality (KORUS-AQ) experiment in South Korea and the Air chemistry Research In Asia (ARIAs) in the North China Plain (NCP). For reference, multispectral CO retrievals (V8J) from the Measurements of Pollution in the Troposphere (MOPITT) are jointly assimilated with meteorological observations using an Ensemble Adjustment Kalman Filter (EAKF) within the global Community Atmosphere Model with Chemistry (CAM-chem) and the

Data Assimilation Research Testbed (DART). With regard to KORUS-AQ data, CO is underestimated by 42 % in the Control-Run and by 12 % with the MOPITT assimilation run. The inversion suggests an underestimation of anthropogenic CO sources in many regions, by up to 80 % for Northern China, with large increments over the Liaoning province and the North China Plains (NCP). Yet, an often-overlooked aspect of these inversions is that correcting the underestimation in anthropogenic CO emissions also improves the comparison with observational O_3 datasets, and observationally constrained box model simulations of OH and HO_2. Running a CAM-chem simulation with the updated emissions of anthropogenic CO reduces the bias by 29 % for CO, 18 % for ozone, 11 % for HO_2 and 27 % for OH. Longer lived anthropogenic VOCs whose model errors are correlated with CO are also improved while short-lived VOCs, including formaldehyde, are difficult to constrain solely by assimilating satellite retrievals of CO. During an anticyclonic episode, better simulation of O_3, with an average underestimation of 5.5 ppbv and a reduction in the bias of surface formaldehyde and oxygenated VOCs can be achieved by separately increasing by a factor of two the modeled biogenic emissions for the plant functional types found in Korea. Results also suggest that controlling VOC and CO emissions, in addition to wide spread NOx controls, can improve ozone pollution over East Asia.

1 Introduction

Carbon monoxide (CO) is a good tracer of biomass burning (Crutzen et al., 1979; Edwards et al., 2004; Edwards et al., 2006) and anthropogenic emission sources (e.g. Borsdorff et al., 2019). It is also the main sink of the hydroxyl radical (OH) and therefore is important in quantifying the methane (CH_4) sink in the troposphere (Myhre et al., 2013; Gaubert et al., 2016, 2017; Nguyen et al., 2020). In fact, because of the lack of observational constraints on the OH spatio-temporal variability, uncertainties in the atmospheric CH_4 lifetime and its interannual variability have precluded accurately closing the global CH_4 budget (Saunois et al., 2016; Prather & Holmes, 2017; Turner et al., 2019). There is a need to reduce uncertainties in the main drivers of OH (National Academies of Sciences, Engineering, and Medicine 2016), which are CO, ozone (O_3), water vapor (H_2O), nitrogen oxides (NO_x), and non-methane volatile organic compounds (NMVOCs).

The evolution of CO in Eulerian chemical-transport is governed for each grid cell by Eq. (1):

$$\frac{\delta CO}{\delta t} = -v \cdot \nabla[CO] + \sum_{i=1}^{Sectors} E_i + \sum_{i=1}^{Chemicals} \chi_i - k[CO][OH] - k_{deposition}[CO] \qquad (1)$$

CO has only one chemical sink, its reaction with OH ($k[CO][OH]$). The other CO sink is dry deposition ($k_{deposition}[CO]$) through soil uptake (Conrad, 1996; Yonemura et al., 2000; Stein et al., 2014, Liu et al., 2018). The direct sources are the emissions from different sectors E_i, the anthropogenic (fossil fuel and biofuel), biomass burning, biogenic and oceanic sources. Locally, CO can be advected from neighboring grid cells ($-v \cdot \nabla[CO]$) and produced from the oxidation of NMVOCs (χ_i). Globally, the oxidation of CH_4 is the main source of chemically produced CO. Biogenic and anthropogenic NMVOCs also contribute significantly to secondary CO.

The use of inverse models and chemical data assimilation systems has helped in constraining the global CO budget and associated trends at global to continental scales, particularly with the availability of long time series of CO retrievals from the Measurement of Pollution In the Troposphere (MOPITT, Worden et al., 2013) satellite instrument (e.g., Arellano et al., 2004; Pétron et al., 2004; Heald et al. 2004; Kopacz et al., 2010; Fortems-Cheiney et al., 2011; Yumimoto et al., 2014). Such studies are generally in agreement with regards to the decreasing long-term

trends in CO emissions from anthropogenic and biomass burning sources (Jiang et al. 2015; Yin et al., 2015; Miyazaki et al. 2017; Zheng et al., 2019), although regional emissions remain largely uncertain. Outstanding issues reported in the literature that still need to be resolved include errors in model transport (Arellano and Hess 2006; Jiang et al. 2013), lack of accurate representation of the atmospheric vertical structure of CO (Jiang et al., 2015), OH fields (Jiang et al., 2011; Müller et al., 2018), aggregation errors (Stavrakou and Müller, 2006; Kopacz et al., 2009), and inclusion of chemical feedbacks (Gaubert et al., 2016). Recent studies have suggested mitigating these issues by assimilating multiple datasets of chemical observations (Pison et al. 2009; Fortems-Cheiney et al. 2012; Kopacz et al., 2010; Miyazaki et al., 2012; Miyazaki et al., 2015), and the use of different models that use the same data assimilation system (Miyazaki et al., 2020a).

Regionally, comparison with in-situ observations of forward and inverse modeling approaches suggests that several standard inventories of CO emissions in China are too low (e.g. Kong et al., 2020; Feng et al., 2020). Recently, Kong et al. (2020) compared a suite of 13 regional model simulations with surface observations over the North China Plain (NCP) and Pearl River Delta (PRD) and found a severe underestimation of CO, despite the models using the most up-to-date emissions inventory, the mosaic Asian anthropogenic emission inventory (MIX) (Li et al., 2017). Using surface CO observations in China, Feng et al. (2020) performed an inversion of the MIX inventory and found posterior emissions that were much higher than the priors, with regional differences, still pointing to a large underestimation in northern China. The large posterior increase of CO emissions in northern China seems to be due to a severe underestimation of residential coal combustion for heating and potentially for cooking (Chen et al., 2017; Cheng M., et al., 2017; Zhi et al., 2017).

While the general underestimation of fossil fuel burning in East Asia seems to explain the underestimation of Northern Hemisphere (NH) extratropical CO found in global models (Shindell et al., 2006), there are other confounding factors. Naik et al. (2013) found large inter-model variability in the regional distribution of OH and an overestimation of OH in the NH. This is consistent with an overestimation of ozone (Young et al. 2013), which provides another explanation of the CO underestimation. Strode et al. (2015) confirmed that the springtime low bias in CO is likely due to a bias in OH. This can be caused by a bias in ozone and water vapor, which are OH precursors. Yan et al. (2014) suggested that these biases could be mitigated by increasing the horizontal resolution within a 2-way nested model. Stein et al. (2014) suggested that anthropogenic CO and NMVOCs from road traffic emissions were too low in their inventory, but also suggested that a wintertime increase in CO could be due to a reduced deposition flux. Secondary CO originating from the oxidation of CH_4 and NMVOCs could also play a role in the CO underestimation (e.g. Gaubert et al., 2016).

Due to significant efforts in reducing emissions in China, including effective implementation of clean air policies which started in 2010 (e.g. Zheng et al., 2018), there has been a reduction of CO emissions of around 27 % since 2010. Bhardwaj et al. (2019) found a decrease of surface MOPITT CO by around 10 % over the NCP and South Korea during the 2007-2016 period. As opposed to NOx emissions that have been decreasing since 2010, inventories suggest a net NMVOCs emissions increase (Zheng et al., 2018). While there are regional differences and no trends were observed in satellite retrievals of CH_2O for the period 2004 to 2014 over Beijing and in the PRD (De Smedt et al., 2015), a more recent study suggests an overall increase of VOC emissions in the NCP by ~25 % between 2010 and 2016 (Souri et al., 2020). Shen et al., (2019) show that CH_2O columns have a positive trend in urban regions of China from 2005 to 2016. Li, M. et al. (2019) found an increase in NMVOCs emissions from the industry sector and solvent use while emissions

from the residential and transportation sectors declined, leading to a net increase in emissions of NMVOCs. A modeling study suggests that the reduction of aerosols over northern China has reduced the sink of hydroperoxyl radicals (HO_2) which resulted in an increase in surface O_3 concentrations in North Eastern China (Li, K. et al., 2019). The transport of ozone pollution between source regions makes it difficult to correlate trends in ozone with the trends in emissions of its precursors (Wang et al., 2017).

Emissions from East Asia are known to impact regional air quality (AQ), and contribute significantly to surface O_3 pollution at regional, continental and even intercontinental scales through trans-Pacific transport, in particular in spring when meteorological conditions favor rapid transport (Akimoto et al., 1996; Jacob et al., 1999; Wilkening et al., 2000; Heald et al., 2006). Frontal lifting in warm conveyor belts (WCBs) efficiently contributes to the transport of pollution (Cooper et al. 2004; Zhang et al. 2008; Lin et al. 2012), which can be observed by satellite retrievals of tropospheric O_3 (Foret et al., 2014) and aircraft in-situ measurements (Ding et al. 2015). However, the mechanisms that cause the uplifted pollution to effectively descend to the downwind surface layers at regional, continental and intercontinental scales are complex. In the case of South Korea, one efficient mechanism could be that once lifted from the emission sources in China, the higher altitude plumes can pass through the marine atmosphere of the Yellow Sea without removal processes such as dry deposition, and reach the surface of the Korean peninsula during the day, when the boundary layer is high (Lee et al., 2019a; Lee et al., 2019b). In addition, severe pollution episodes can be due to local emissions under stagnant conditions with reduced regional ventilation and lower wind speed (Kim et al. 2017).

The recent literature and findings from the 2016 field campaign over South Korea indicate the relative importance of O_3 precursors and associated transport in this region. The Korea-United States Air Quality (KORUS-AQ) field campaign was a joint effort between the National Aeronautics and Space Administration (NASA) of the United States and the National Institute of Environmental Research (NIER) of South Korea. The field campaign's objective was to quantify the drivers of AQ over the Korean Peninsula with a focus on the Seoul Metropolitan Area (SMA), currently one of the largest cities in the world. The intensive measurement period was from May 1 2016 and June 15 2016 with the deployment of a research vessel (Thompson et al., 2019) and 4 different aircraft: the NASA DC-8, the NASA B200, the Hanseo University King Air and the Korean Meteorological Agency (KMA) King Air. The aircraft sampled numerous vertical profiles of trace gases, aerosols and atmospheric physical parameters with missed approach flying procedure over the SMA (e.g. Nault et al., 2018) and spiral patterns over the Taehwa Research Forest (TRF) site, downwind from the SMA (e.g. Sullivan et al., 2019). Peterson et al. (2019) studied the weather patterns during KORUS-AQ and distinguished four distinct periods defined by different synoptic patterns: a dynamic meteorological phase with complex aerosol vertical profiles, a stagnation phase with weaker winds, a phase of efficient long-range transport, and a blocking pattern.

This campaign provides several case studies of foreign-influenced and local pollution episodes. Miyazaki et al. (2019a) assimilated a suite of satellite remote sensing of chemical observations and found that under dynamic conditions, when there was efficient transport with uplifting of pollution to higher altitudes (where the satellite has more sensitivity), forecasted ozone was improved by the assimilation of satellite ozone retrievals. On the contrary, under stagnant conditions, forecasted ozone was not improved as much when compared to the DC-8 ozone measurements, suggesting ozone formation closer to the surface. Lamb et al. (2018) studied at the vertical distribution of black carbon during KORUS-AQ. Aside from a short episode of biomass burning sources from

Siberia, they found that the Korean emissions were important in the boundary layer, with a large contribution from long-range transport from mainland China that varies with the large-scale weather patterns. There are different ways to quantify the sources contributing to pollutants, such as Lagrangian back trajectory, VOCs signatures, CO to CO_2 ratios and CO "tags" (Tang et al., 2019). Overall, direct Korean CO emissions are important contributors to the boundary layer CO, but not higher up where emissions from continental Asia dominate. Simpson et al. (2020) performed a source apportionment of the VOCs over the SMA and also found a significant source of CO from long-range transport with only a smaller CO source from combustion over Seoul. Since long-range transport is important, the forecasted CO and water vapor during KORUS-AQ can be improved by assimilating Soil Moisture from the NASA SMAP satellite (Soil Moisture Active Passive) over China (Huang et al, 2018). They stress the importance of error sources stemming from chemical initial and boundary conditions and emissions for modeling CO during two studied pollution events.

While chemical data assimilation is effective for CO in a global model, because of its longer lifetime than most of the reactive species, there are some limitations if the parameters, such as emissions inventories inputs or physical and chemical processes, are not updated consistently with the initial conditions (Tang et al., 2013). The KORUS-AQ campaign provides a large array of measurements and is an excellent case study for testing the model with challenges that need to be addressed for further improvements of CO and related species of interest such as OH, O_3, CH_4 and NMVOCs. Here we take advantage of the concurrent measurements during the campaign to investigate the reasons for the CO underestimation and we attempt to answer the following question: Can we explain why CO is consistently underestimated over East Asia, using a Chemical Transport Model, field campaigns and satellite data assimilation?

We outline the set of observations used to verify and evaluate our chemical data assimilation system in Section 2. The modeling system is presented in Section 3, the Data Assimilation system in Section 4, the evaluation of the data assimilation results in Section 5. The comparison of emissions estimates and additional sensitivity experiments in Section 6.

2 Field campaign observations

2.1 The Korea United States Air Quality (KORUS-AQ) field campaign

The KORUS-AQ campaign provides a unique testbed for comparing surface and aircraft in-situ observations with ground-based and satellite-based remote sensing (Herman et al. 2018), particularly important for the targeted short-lived species such as formaldehyde (CH_2O) and nitrogen dioxide (NO_2). Miyazaki et al. (2019a) showed that the background O_3 measured by the DC-8 during KORUS-AQ ranges from 72 to 85 ppbv between the surface and 800 hPa over the Korean Peninsula. On top of these large background values, large emissions from the SMA are responsible for the strong formation of secondary organic aerosols (Kim et al., 2018; Nault et al., 2018) and O_3, which can be further enhanced by biogenic emissions eastward of Seoul (Sullivan et al., 2019). Large ozone production is a result of emissions from areas characterized to be VOC-limited, such as the urbanized SMA and industrialized regions into a NO_x-limited environment over rural and forested regions. Both Oak et al. (2020) and Schroeder et al. (2020) examined O_3 production during KORUS-AQ with a focus on the SMA and surrounding regions and reported a higher ozone production efficiency over the rural areas. They pointed out higher ozone sensitivity to aromatics, followed by isoprene and alkenes. Observations over the Taehwa Research Forest

east of Seoul show strong ozone production (Kim et al., 2013) because of large emissions of reactive biogenic VOCs, in particular isoprene and monoterpenes.
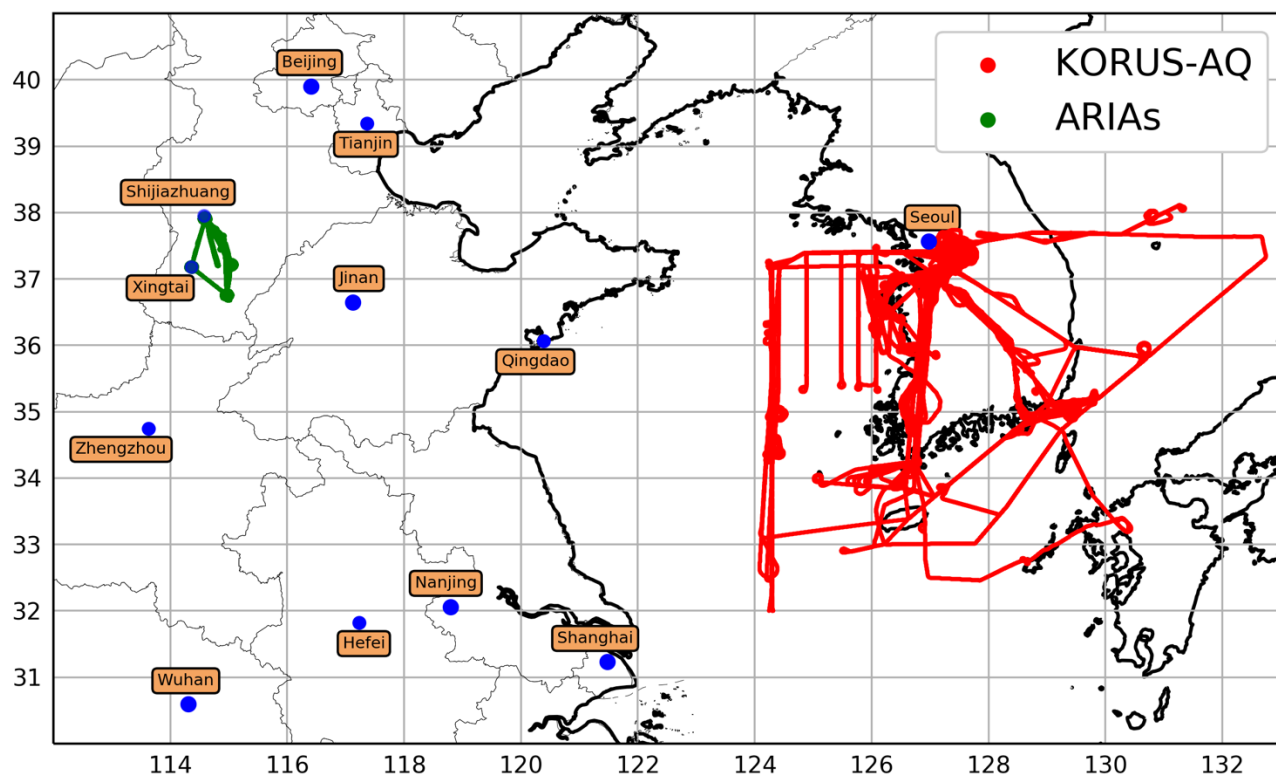
Figure 1: Location of all the KORUS-AQ DC-8 1-min merge measurements (red dots), and of the ARIAs Y-12 1-min merge measurements (green dots). The location of some major cities is also indicated (blue dots).

We evaluate the model output against the DC-8 aircraft measurements, shown in red in Figure 1, which simultaneously provide many physical and chemical parameters of the tropospheric chemistry environment system (appendix A). We use the 1-minute merge file of DC-8 in-situ observations. Model outputs were linearly interpolated to the exact location of the DC-8 in latitude, longitude, pressure altitude and in time, from the 6 hourly model outputs. During the whole campaign, Simpson et al. (2020) showed that high benzene concentrations (> 1 ppbv) were only found close to the Daesan petrochemical complex. Since those large gradients of local plumes simply cannot be modeled in a global model, we systematically rejected observations when the benzene proton-transfer-reaction time-of-flight mass spectrometer (PTR-ToF-MS) measurements were higher than 1 ppb.

In order to evaluate the CO sink and the impact of the assimilation of MOPITT CO retrievals on the HO_x levels, we used the OH and HO_2 calculated with the NASA Langley Research Center (LaRC) 0-D time-dependent photochemical box model (Schroeder et al., 2020). This box model is constrained by measured temperature and pressure, photolysis rates derived from actinic flux observation and observations of O_3, NO, CO, CH_4, CH_2O, PAN, H_2O_2, water vapor, and non-methane hydrocarbons. The production and loss terms of ozone is calculated for every single 1 Hz DC-8 set of observations. This is the only case where we use the 1-second merge file instead of the 1-min merge dataset file. CAM-chem outputs are interpolated accordingly. While there are some limitations for the species with longer lifetimes, subject to physical processes that are not

represented, the box model has been specifically designed to estimate radical concentrations. The details and sensitivity of the calculation are described in Schroeder et al. (2020).

2.2 The ARIAs campaign

The Air Chemistry Research In Asia (ARIAs) field campaign was conducted in May and June 2016 with the goal of better quantifying and characterizing air quality over the NCP (Benish et al., 2020; Wang et al. 2018). The instrumented Y-12 airplane was operated by the Weather Modification Office of the Hebei Province to measure meteorological parameters, aerosols optical properties and trace gases. The airplane was based in Luancheng Airport, southeast of Shijiazhuang, the capital of Hebei Province, and flew vertical spirals from ~300m to ~3500 m over the cities of Julu, Quzhou, and Xingtai (Fig. 1). There were 11 research fights between May 8, 2016 and June 11, 2016. Wang et al. (2018) identified three different Planetary Boundary Layer (PBL) structures with distinct aerosol vertical structure. The aerosol pollution was mostly located below an altitude of 2 km, but sometimes with a vertically inhomogeneous structure, with higher aerosols at higher altitudes than at the surface but still in the boundary layer. These vertical structures were mostly observed when the pollution originated from the southwest and from the eastern coastal region of the study domain, while cleaner air masses originated from the northwest. CO was measured by Cavity Ring Down Spectroscopy by the Picarro Model G2401-m instrument with a 5-second precision of 4 ppbv and an estimated accuracy of ±1% and O_3 by UV-absorption using a Thermal Electron Model 49C ozone analyzer. O_3 values ranged from 52 ppbv to 142 ppbv, partly because flight days were chosen to target meteorological conditions favorable to smog events (Benish et al., 2020). CO concentrations ranged from 91 ppbv to about 2 ppmv (Benish et al., 2020). The pervasive high levels of CO correlated with SO_2 indicate extensive low-tech coal combustion. We rejected individual CO observations (about 5% of total CO observations) when SO_2 was greater than 20 ppbv (the 95th percentile of all observations) to remove the extremely polluted plumes.

3 Model configuration and improvements

3.1 Community Atmosphere Model with Chemistry (CAM-chem)

We use the open-source Community Earth System Model version 2.1 (CESM2.1); an overview of the modeling system and its evaluation is presented in Danabasoglu et al. (2020). It contains many new scientific features and capabilities, including an updated coupler, the Common Infrastructure for Modeling the Earth (CIME), which allows for running an ensemble of CESM runs, in parallel with a single executable. The atmosphere is modeled using the finite volume dynamical core of the Community Atmosphere Model version 6 (CAM6) with 32 vertical levels and a model top at 3.6 hPa, and a 1.25° (in longitude) by 0.95° (in latitude) horizontal resolution (Gettelman et al., 2019). The model now uses a unified parameterization of the planetary boundary layer (PBL) and shallow convection, the Cloud Layers Unified by Binormals (CLUBB, Bogenschutz et al. 2013). Other updates on the model physical parameterizations are described in Gettelman et al. (2019). The new Troposphere and Stratosphere (TS1) reduced gas phase chemical mechanism contains 221 species and 528 reactions (Emmons et al., 2020), and thus explicitly represents stratospheric and tropospheric ozone and OH chemistry. This chemical scheme contains many updates, including on the isoprene oxidation mechanism, splitting a single aromatic into BENZENE, TOLUENE and XYLENES lumped species and a terpene speciation. The overall setup of CESM2.1 has been updated following the protocol of the Coupled Model Intercomparison Project Phase 6, which includes solar forcings (Matthes et al., 2017), surface greenhouse gases boundary

conditions (Meinshausen et al., 2017) and anthropogenic emissions. Therefore, we use the anthropogenic emission inventory of chemically reactive gases that has been generated by the Community Emissions Data System (CEDS, Hoesly et al., 2018). We use the latest year available (2014) for the KORUS-AQ period (2016). It is commonly acknowledged that errors in the emission inventory for China are much larger than the trends between different years (Feng et al., 2020). Anthropogenic emissions over East Asia are replaced by the KORUS inventories version 5 or KORUS v5, based on the Comprehensive Regional Emissions for Atmospheric Transport Experiment (CREATE) (Woo et al., 2012). Daily Biomass Burning emissions are obtained from the Fire Inventory from NCAR (FINN v1.5) version 1.5 (Wiedinmyer et al., 2011). Biogenic emissions are modeled within the Community Land Model, using the algorithms of the Model of Emissions of Gases and Aerosols from Nature (MEGAN v2.1) (Guenther et al., 2012). A summary of the model references is presented in Table 1. We have made some additional changes for this study, presented in Appendix B. In particular, we updated the heterogeneous uptake coefficient of HO_2 and its coefficient.

Table 1: Summary of the main model components and references for CESM2.1 / CAM6-Chem.

Model component	Reference
Community Earth System Model Version 2.1 (CESM2.1)	Danabasoglu et al., 2020
Community Atmosphere Model version 6 (CAM6)	Gettelman et al., 2019
Tropospheric and Stratospheric chemistry scheme (TS1)	Emmons et al., 2020
Organic aerosol scheme (with Volatility Basis Set)	Tilmes et al., 2019
Modal Aerosol Module (MAM4)	Liu et al., 2016
Community Land Model (version 5)	Lawrence et al., 2019
Model of Emissions of Gases and Aerosols from Nature (version 2.1)	Guenther et al., 2012
Inputs	
Community Emissions Data System (CEDS)	Hoesly et al., 2018
Comprehensive Regional Emissions for Atmospheric Transport Experiment (CREATE) version 5 or KORUS v5	Woo et al., 2012
Fire Inventory from NCAR (FINN v1.5) version 1.5	Wiedinmyer et al., 2011
Greenhouse gases prescribed fields	Meinshausen et al., 2017
Methane net surface fluxes	Saunois et al., 2020

3.2 Sensitivity test on the biogenic emissions

The KORUS-AQ campaign was subject to photochemical episodes with large concentrations of secondary aerosols and ozone (e.g. Kim H. et al., 2018). There is a significant amount of biogenic emissions from the South Korean forests including deciduous oak trees (Lim et al., 2011) and conifers such as the Korean pine (Pinus koraiensis), both of which surround the Taehwa Research Forest site. As a result, there are large emissions from a variety of compounds, such as isoprene, monoterpenes and sesquiterpenes, which contribute to enhanced ozone in favorable conditions (Kim S. Y. et al., 2013; Kim S. et al., 2015, 2016; Kim H.-K et al., 2018). Oak et al. (2020) showed that the largest ozone production efficiency was in the rural areas of South Korea, where biogenic emissions are dominant. Kim et al. (2014) studied how the Plant Functional Type (PFT) distributions affect the results of biogenic emission: broadleaf trees, needleleaf trees, shrub, and herbaceous plants are significant contributors to BVOCs in South Korea. They found large sensitivities of calculated biogenic emissions to 3 different PFT datasets over Seoul, which resulted

in local but significant changes in simulated O_3. We performed a sensitivity analysis to the biogenic emissions by increasing the emission factors for three of the Community Land Model PFT that are present in Korea, the "Needleleaf Evergreen Temperate Tree", the "Broadleaf Evergreen Temperate Tree", and the "Broadleaf Deciduous Temperate Tree". We perform a set of simulations by varying biogenic emissions to determine the best fit to the observations of formaldehyde (CH_2O) at the surface (see SI). For the sake of clarity, we will present one experiment denoted as CAM_MOP-Bio (see Sect. 4.6).

4. Chemical data assimilation system

4.1 Data Assimilation Research Testbed (DART) implementation

The Data Assimilation Research Testbed (DART) is an open source community facility for ensemble data assimilation developed and maintained at the National Center for Atmospheric Research (Anderson et al., 2009a). DART has been used in numerous studies for Data Assimilation (DA) within CESM (Hurrell et al., 2012, Danabasoglu et al., 2020). Global DA analyses have been carried out with assimilation of conventional meteorological datasets within the Community Atmosphere Model (CAM, Raeder et al. 2012), the Community Land Model version 4.5 or CLM4.5 (Fox et al. 2018), and in a weakly coupled atmospheric assimilation in CAM and oceanic assimilation in the Parallel Ocean Program ocean model (Karspeck et al. 2018). The Chemical Data Assimilation system inherits from previous work that coupled the Ensemble Adjustment Kalman Filter (EAKF) analysis algorithm (Anderson et al., 2001) with CAM-chem. The DART/CAM-chem is designed for efficient ensemble data assimilation of chemical and meteorological observations at the global scale (Arellano et al., 2007; Barré et al., 2015; Gaubert et al., 2016, 2017).

4.2 DART/CAM-chem analysis and forecast algorithm

The analysis is carried out using a deterministic ensemble square root filter, the Ensemble Adjustment Kalman Filter (EAKF) (Anderson 2001, 2003). The ensemble of 30 CAM-chem members is run with a single executable of CESM using the multi-instance capability. At the analysis step, the following model variables are updated when weather observations are assimilated: surface pressure, temperature, wind components, specific humidity, cloud liquid water and cloud ice. Assimilated observations include radiosondes, Aircraft Communication, Addressing, and Reporting System (ACARS), but also remotely sensed data including satellite drift winds and Global Positioning System (GPS) Radio Occultation. We use a similar setup as previous studies (Barré et al., 2015; Gaubert et al., 2016, 2017) with a spatial localization of 0.1 radians or ~600 km in the horizontal and 200 hPa in the vertical for both chemical and meteorological observations. We now use the spatially and temporally varying adaptive inflation enhanced algorithm (El Gharamti 2018), that generalizes the scheme of Anderson (2009b). Multiplicative covariance inflation is applied to the forecast ensemble before each analysis step.

4.3 MOPITT assimilation

As in previous implementations, both CO retrievals from MOPITT and meteorological observations are simultaneously assimilated within the DART framework. We assimilate profiles of retrieved CO from the MOPITT nadir sounding instrument onboard the NASA Terra satellite. The MOPITT V8J product (Deeter et al., 2019) is a multispectral retrieval using the CO absorption in the Thermal Infra-Red (TIR, 4.7 μm) and Near Infra-Red (NIR, 2.3 μm) bands (Worden et al.,

2010). The objective is to maximize the retrieval sensitivity to the lower layers of the atmosphere while minimizing the bias. We apply the same filtering thresholds that are used to create the L3 TIR-NIR product, which exclude all observations from Pixel 3 in addition to observations where both (1) the 5A signal to noise ratio (SNR) is lower than 1000 and (2) the 6A SNR is lower than 400. We apply the strictest retrieval anomaly flags (all from 1 to 5). We only assimilate daytime measurements, where latitudes are lower than 80 degrees and when the total column degrees of freedom are higher than 0.5. Super-observations are produced by applying an error-weighted average of the profiles (Barré et al., 2015) on the CAM-chem grid, with no error correlation since we consider those to be minimized by a strict use of the quality flags, as in Gaubert et al. (2016). In general, MOPITT data have errors smaller than 10% (Tang et al., 2020; Hedelius et al., 2019), which is much lower than model errors. We evaluate our assimilation results with fully independent aircraft observations.

4.4 Ensemble design

The ensemble of prior emissions is generated by applying a spatially and temporally correlated noise to the given prior emission field, as in previous studies (Gaubert et al., 2014, 2016, 2017; Barré et al., 2015, 2016). Emission perturbations are generated from a two-dimensional Gaussian distribution with zero mean and unitary variance (Evensen, 2003), with a fixed spatial correlation length. Here we applied the same set of perturbations for every time step, thus the prior ensemble has a temporal correlation of 1. A different noise distribution is drawn for Biomass Burning (BB) CO emissions than for anthropogenic direct CO emissions, with a decorrelation length of 250 km for BB, and 500 km for direct anthropogenic CO. Thus, as opposed to the previous studies, anthropogenic and BB CO sources are completely uncorrelated in the prior ensemble. The same noise is then applied to all the species emitted by the same source, BB or anthropogenic, including NMVOCs, the non-organic nitrogen species, SO_2, and aerosols. This means the added noise in emissions of NMVOCs and CO from the BB or anthropogenic sectors will be completely correlated. We generated another noise sample with a decorrelation length of 500 km for soil emissions of NO.

The ensemble spread in the model physics variables is important for CO, which is directly sensitive to errors in horizontal and vertical winds (both boundary layer height and convection), as well as surface exchange, and indirectly through the impact of dynamics and physics on other chemicals. In particular, a spread in the MEGAN estimates of direct and indirect CO emissions from biogenic sources will be generated from the different atmospheric states passed to the land model. We assigned a spatially and temporally uniform noise drawn from a normal distribution with a standard deviation of 0.1 to the CH_4 emissions. More work will be done to generate a realistic spread in CH_4 emissions, but that is beyond the scope of this study. The ensemble spin-up starts on April 1 2016 with perturbed emissions described above and with a spread in nudging parameters to perturb the dynamics. After a week, on April 7 2016, the Control-Run ensemble is initialized from the spin-up, this simulation is not nudged and this period is used to spin-up the inflation parameters for the assimilation of the weather observations only. The MOPITT-DA run is initialized from the Control-Run ensemble on April 15 2016.

4.5 Variable localization and parameter estimation

The multivariate error background error covariance allows for an estimation of the error correlation between the adjusted model variables or state vector and observations. As in previous studies we choose a strict "variable localization" (e.g. Kang et al., 2011), because (1) it is easier to quantify the impacts of the assimilation, such as the chemical response (Gaubert et al., 2016), as well as the

model and observations errors (Gaubert et al., 2014); (2) spurious correlation can have a strong impact on the non-assimilated species that have no constraints. This strict variable localization means that the assimilation of MOPITT only corrects the chemical state vector (i.e. CO) and has no impact on the meteorological state vector (U, V, T, Q, Ps) and vice-versa. However, we made an exception and extended our chemical state vector by including CO emissions from BB and anthropogenic sources separately and several NMVOCs. We added C2H2, C2H4, C2H6, C3H8, benzene, toluene, and the XYLENES, BIGENE and BIGALK surrogate species to the state vector. The NMVOCs with a strong anthropogenic and/or BB origin that have a primary sink with OH should be strongly correlated with CO (Miyazaki et al., 2012). The relationships between NMVOCs and CO leads to a correlation in their errors, so that the correlation existing in the ensemble will reflect those true errors. In addition to the initial spread described above, spatially and temporally varying adaptive inflation is also applied to the optimized CO Surface Flux (SFCO) model variable during the analysis procedure.

In CAM-chem, a diurnal profile is not applied to the emissions, instead emissions are interpolated from the dates provided in the inventories, which is daily for BB and monthly for anthropogenic sources. The relative increments obtained from the analysis in the form of the surface fluxes model variable (SFCO) is propagated back to the input files emissions (E) following:

$$E_i^{analysis} = E_i^{prior}(1 + w\frac{\Delta SFCO_i}{SFCO_i}) \tag{2}$$

where i is an ensemble member and $w = a\,e^{-\frac{t}{\tau}}$ is a weight to represent the temporal representativeness and to limit the impact of spurious correlation. At the analysis time (t=0), the weight will be w=a, with a=0.8, i.e. 80 % of the initial increments in Eq. 2. For the other time steps t, the exponential decay characteristic time, τ, is set to 4 days in the case of BB and 4 months in the case of anthropogenic emissions. The impact of the increments will therefore decrease exponentially for the other time steps t from 0.8 to 0, which is imposed (bounded) for 2τ (8 months or 8 days). This makes a strong correction for the current time and the closest time step. This allows for smoothing the increments over time while hopefully leading to a convergence through the sequential correction of the emissions during the assimilation run.

4.6 Simulations overview

In section 5, two simulations with the assimilation of meteorological observations will be presented, the Control-Run and the MOPITT-DA and the difference between the two simulations is the assimilation of MOPITT in the MOPITT-DA run. In the MOPITT-DA assimilation run, the initial conditions of CO and some NMVOCs, and CO emission inventories from anthropogenic and biomass burning sources, are optimized during the analysis step. The summary of the simulations presented in the following sections is presented in Table 2.

In section 6, we compare our emission estimates with a state-of-the-art chemical data assimilation and inversion system, the Tropospheric Chemistry Reanalysis version 2 or TCR-2 (Miyazaki et al., 2019b, Miyazaki et al., 2020b). They assimilate a variety of satellite instruments using the Local Ensemble Transform Kalman Filter (LETKF, Hunt et al. 2007) with the MIROC-chem model (Wanatabe et al. 2011). The setup is fully described and evaluated in Miyazaki et al. (2020b). We regridded the anthropogenic prior and posterior CO estimate from their 1.125° × 1.125° mesh grid to the CAM-chem grid. In the TCR-2, the prior anthropogenic emission is HTAP v2 for 2010 (Janssens-Maenhout et al., 2015).

Additional sensitivity tests will be performed using deterministic CAM-chem simulations (Table 2) and presented in section 7. In this case, since no meteorological data assimilation is performed,

the dynamics from the prognostic variables U, V, and T need to be nudged towards the NASA GMAO GEOS5.12 meteorological analysis in order to reproduce the meteorological variability. The GEOS analysis is first regridded on the CAM-chem horizontal and vertical mesh. The nudging is driven by two factors: the strength, a normalized coefficient that ranges between 0 and 1; and the frequency of the nudging, here configured to use 6-hourly outputs from either the GEOS5 reanalysis or our own DART CAM-chem Control-Run. Based on an ensemble of sensitivity tests (SI), we use the nudging setup that minimizes the meteorological errors for the KORUS-AQ observations. This best simulation is the g-post-0.72, hereafter denoted as CAM_Kv5 (Table 2), and will serve as a reference for the additional sensitivity simulation experiments. Aside from the Control-Run and the MOPITT-DA, the CAM-chem simulations have the same nudging setup, and only differ by the CO anthropogenic emissions flux. In addition, the CAM_MOP-Bio is the same as the CAM_MOP but with an overall increase in the MEGAN emission factor. Note that the simulations denoted as CAM_HTAP (TCR-2 Prior) and CAM_TCR-2 (TCR-2 Posterior) are CAM-Chem simulations with the respective anthropogenic CO emissions from TCR-2. We also use the Copernicus Atmosphere Monitoring Service (CAMS) global bottom-up emission inventory (Granier et al. 2019; Elguindi et al., 2020). We use the CAMS-GLOB-ANTv3.1, which has only minor changes with regards to the most recent version (v4.2). The gridded inventory is available at a spatial resolution of $0.1° \times 0.1°$ and at a monthly temporal resolution for the years 2000-2020. It is built on the EDGARv4.3.2 annual emissions (Crippa et al., 2018) and extrapolated to the most current years using linear trends fit to the years 2011-2014 from the CEDS global inventory. We included artificial CO tracers or "CO tags", to track the anthropogenic contribution from different geographic area sources (e.g., Gaubert et al., 2016).

Table 2: Summary of the simulations. The Nudging (GEOS) refers to a CAM-Chem deterministic runs with specified dynamics, using a nudging to GEOS-FP analysis winds and temperatures (see supplement). Aside from the DART simulations (first 2 rows), all the simulations have the same initial conditions and the same nudging and only change by their anthropogenic CO emissions inputs.

Simulation name	Meteorology	Emissions (prior)
Control-Run	Assimilation (DART)	Prior (CEDS-KORUS-v5)
MOPITT-DA	Assimilation (DART)	Optimized (CEDS-KORUS-v5)
CAM_Kv5	Nudging (GEOS)	Prior (CEDS-KORUS-v5)
CAM_HTAP	Nudging (GEOS)	Prior (HTAP v2)
CAM_MOP	Nudging (GEOS)	Posterior (CEDS-KORUS-v5)
CAM_MOP-Bio	Nudging (GEOS)	Posterior (CEDS-KORUS-v5) + MEGANx2 (see SI)
CAM_TCR-2	Nudging (GEOS)	Posterior (TCR-2, HTAP v2)
CAM_CAMS	Nudging (GEOS)	CAMS (CAMS-GLOB-ANTv3.1)

5 Assimilation results: Evaluation of the posterior CO during KORUS-AQ

We use the fully independent DC-8 Differential Absorption CO Measurement (DACOM CO) measurements to evaluate the MOPITT assimilation. Figure 2 compares the averaged vertical profiles for the 4 different mission weather regime phases (Peterson et al., 2019) and the average and standard deviation of all the flights. Observed background CO in the upper free troposphere is between 100 ppbv and 125 ppbv and shows a variation of around 10 % between the different phases. The Control-Run shows an average background between 70 ppbv and 100 ppbv for the four phases and 80 ppbv for the full KORUS-AQ period, while the MOPITT-DA varies between

525   80 ppbv and 110 ppbv for the 4 phases with an average of 90 ppbv for the KORUS-AQ period. The RMSE in MOPITT-DA is reduced by around 10 ppbv compared to the Control-Run for the free troposphere (700 hPa to 300 hPa, Fig. 2).

For the layers closer to the surface, the temporal variations are much stronger. During Phase 3,
530   observed CO is 44 % and 30 % higher than the campaign average at 850 hPa and 950 hPa, respectively. While this feature is much better reproduced after assimilation, absolute RMSE values remain large. Overall, the bias is greatly reduced for the MOPITT-DA in the layers between 850 hPa and 650 hPa. We note that the mean CO is still lower than the average observations. The MOPITT-DA shows at the 950 hPa and 850 hPa levels an underestimation of around 30 ppbv, i.e.
535   between 10 % and 20 % lower than the observations. This is in the range of the expected performance given the retrieval uncertainties (10 %) and the spatial footprints of MOPITT pixels (22km x 22km)
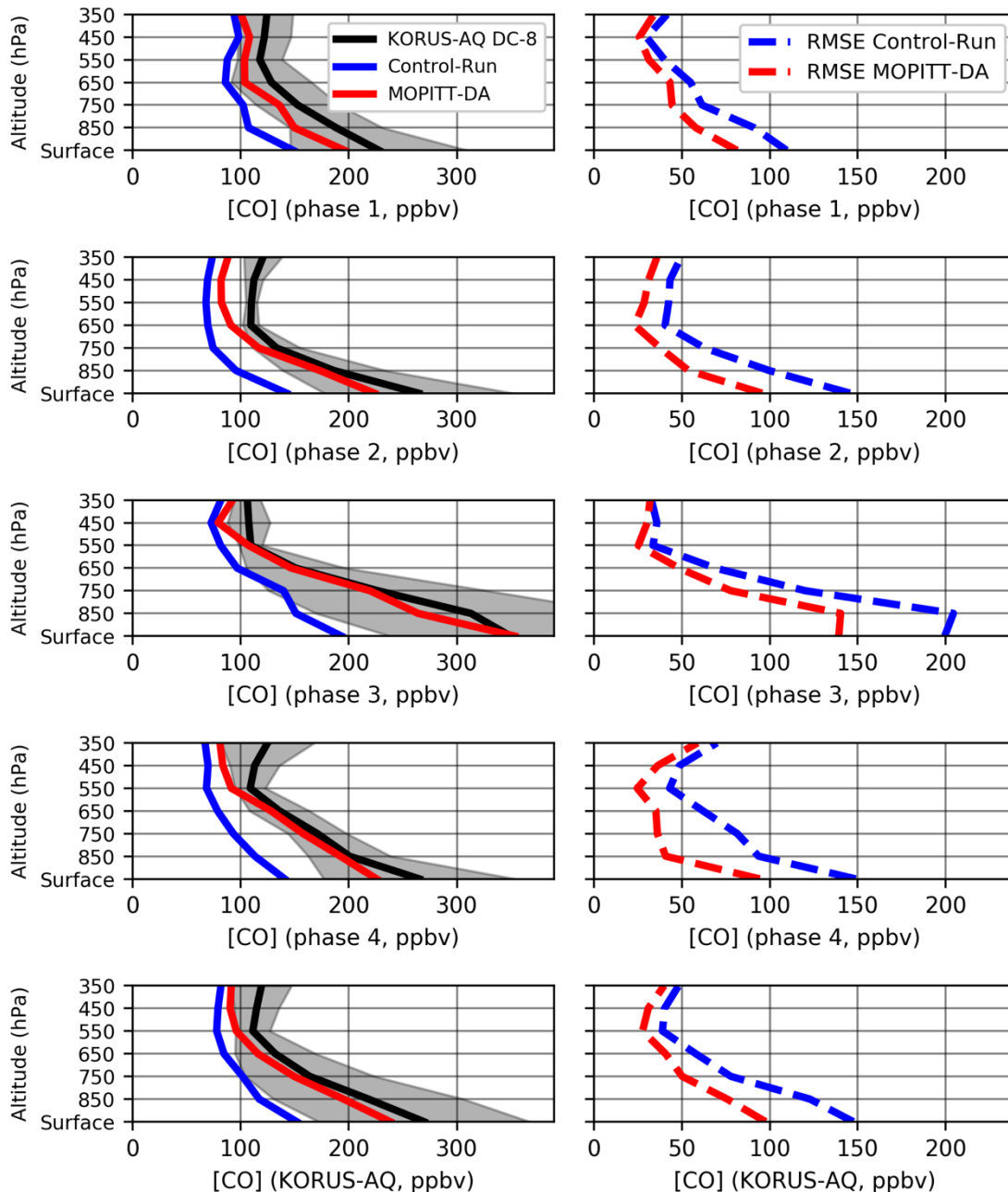
Figure 2: Average CO profiles (left panels) and related RMSE (right panels) for the Control-Run and the MOPITT-DA. The mean (black line) and standard deviation (shaded grey) of the DC-8 observations are calculated for each 100 hPa bin. The first 4 rows are averaged over the different weather regimes of the campaign (Peterson et al. 2019). The last row displays the average over the whole campaign.

5.1 VOCs state vector augmentation

Concentrations of some VOCs have been added to the state vector and are therefore optimized, according to the covariance estimated by the ensemble, when MOPITT observations are assimilated. This setup will only provide meaningful corrections if CO and VOCs errors are highly correlated through common atmospheric and emission processes and if the ensemble samples those errors in the background error covariance. In this case VOCs analysis errors should be reduced by assimilating MOPITT CO, even though VOCs are not directly observed.

Table 3: VOCs added to the state vector, corresponding measuring instrument, and lifetime (Simpson et al., 2020) used for validation. For comparison with surrogate species, the sum of all the corresponding VOC observations is used. WAS stands for Whole Air Sampler.

Model Variable	Observations	Lifetime (days)
C_2H_6	ethane (WAS)	48
C_2H_2	ethyne (WAS)	15
C_3H_8	propane (WAS)	11
BENZENE	benzene (PTRMS)	9.5
BIGALK	i-butane, n-butane, i-pentane, n-pentane, n-hexane, n-heptane, n-octane, n-nonane, n-decane (WAS)	3.5 +/- 1.6
TOLUENE	toluene (PTRMS)	2.1
C_2H_4	ethene (WAS)	1.5
XYLENES	mp-xylene, o-xylene (WAS)	0.7 +/- 0.2
BIGENE	1-butene, i-butene, trans-2-butene, cis-2-butene, 1-3-butadiene (WAS)	0.2 +/- 0.1

The list of optimized VOCs is shown in Table 3, together with their lifetime and the corresponding species from the Whole Air Sampler (WAS) instrument used for evaluation. An increase in concentration is found for all 9 VOCs in the MOPITT-DA simulation, either because of the state augmentation, and/or because of the reduction in OH due to CO adjustments. Even if the changes are small, this can lead to an increase in errors for the vertical profiles compared to observations when the species is already overestimated in the lower layer of the atmosphere. This is the case for C_2H_4 and BIGENE, the only two species that have substantial biogenic and fire sources, as well as for xylenes and toluene. For all the other species, which are underestimated and are mostly from anthropogenic sources, the assimilation leads to an improvement compared to the observations, mostly by reducing their biases. The best results are obtained for ethane and to a lesser extent propane (Fig. 3). Despite the broad anthropogenic source, ethane and propane originate from sectors that are quite different from CO. However, CO, ethane and propane have one thing in common which is that their only atmospheric chemical sink is through OH oxidation. This suggests that a bias in OH leads to correlated errors between CO and alkanes that can be mitigated by including these species to the state vector.

We define a metric of improvement based on the relative change in RMSE that is positive when the RMSE is reduced. Figure 3 shows a clear dependence of this metric on the atmospheric lifetime of the VOCs. All the modeled VOCs with a lifetime shorter than 5 days show an increase in errors, while all the VOCs with a lifetime greater than 10 days are improved, with the largest improvement for ethane, which has a lifetime of 48 days. The relatively large spatial and temporal scales of CO that arise due to its medium atmospheric lifetime significantly limit the ability of CO assimilation to resolve the high-frequency changes in those compounds with short lifetimes. More importantly, this is also to be expected given the limited sensitivity of the MOPITT observations to boundary layer CO.

While satellite observation spatiotemporal resolution and sampling might be improved in the future, NMVOCs with a lifetime shorter than several days should not be included in the state vector when assimilating CO. However, the concentrations of NMVOCs with strong anthropogenic or BB sources and similar chemical characteristics to CO might be significantly improved by the assimilation. We believe that this could also be true for methane.
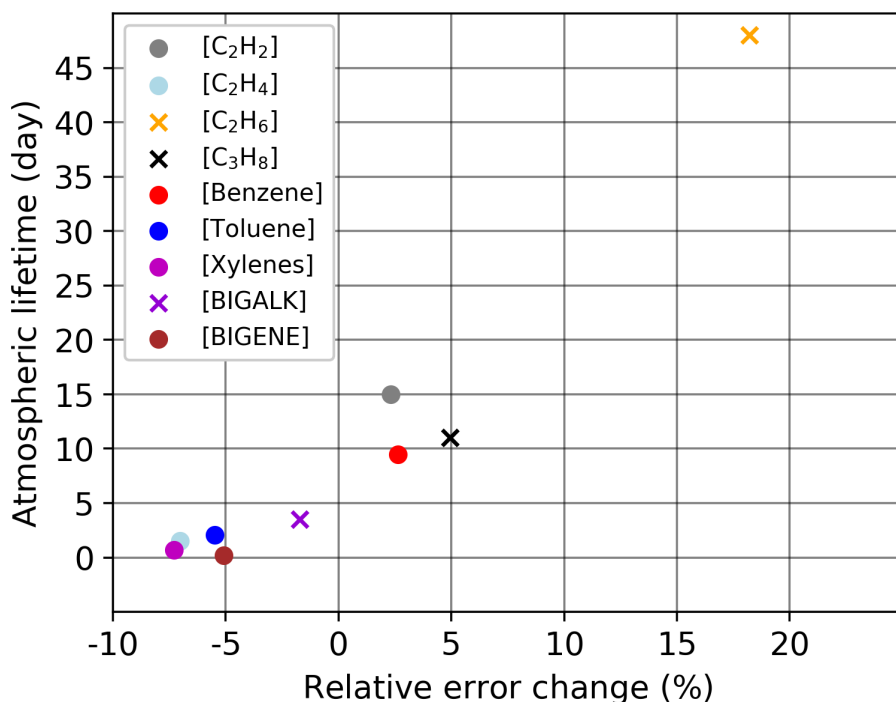
Figure 3: Atmospheric lifetime (from Simpson et al., 2020) in days for the VOCs added to the state vector. Xylenes, BIGALK and BIGENES are surrogate species, so an average of the lifetimes is calculated. The relative error change is the opposite of the difference in Root Mean Square Error relative to the Control-Run (i.e., (Control-Run-MOPITT-DA)/Control-Run). Thus, a positive relative error change means an improvement compared to the Control-Run.

5.2 Chemical response from MOPITT-DA

This section presents a short summary of the impact of the CO assimilation on the chemical state of the atmosphere and the comparison with unobserved species. Figure 4 shows the average vertical profiles for OH, HO_2, NO, NO_2, CH_2O and O_3. We use simulated OH and HO_2 from the observationally constrained NASA LaRC box model (Schroeder et al., 2020). The Control-Run and the LaRC box models agree on the mean OH spanning the first two binned layers, at lower altitudes. Aloft, the Control-Run overestimates the LaRC box model simulations. The Control-Run underestimates HO_2, which suggests that the excellent agreement on OH in the boundary layer is likely caused by compensating errors. That is, the increase of CO through the MOPITT assimilation decreases the OH concentrations (Gaubert et al., 2016). Here, we find better agreement of the model OH with the observationally constrained LaRC box model simulation at 750 hPa and above. This in turn increases HO_2 and shows a better match with the LaRC box model. This suggests that a small part of the HO_2 underestimation can be explained by the CO underestimation. NO and NO_2 are reasonably well modeled for the surface layer, but are underestimated above, with a large underestimation at 850 hPa. Additional comparison with HNO_3, $J(O_3)$, $J(NO_2)$ and H_2O_2 and PAN are shown in Figure S2. The underestimation of NO_x at 850 hPa could be due to the underestimation of NO_x and PAN from upwind source regions. Despite the update of the HO_2 heterogeneous uptake reaction and coefficient presented in appendix B, the CO increase leads to higher levels of H_2O_2, and the bias is therefore higher in the MOPITT-DA than the Control-Run (Figure S2). A lower value of the HO_2 heterogeneous uptake coefficient than the one used here ($\gamma=0.1$) might produce better results by reducing the HO_2 sink (see Appendix

B). It suggests that errors in NO_x and related chemistry drive the underestimation of HO_2 and of the sum of OH and HO_2 (HO_x). Overall, HO_x is underestimated, and OH is fairly well simulated. This suggests that the CO chemical sink alone cannot explain the CO underestimation during the campaign. Alternatively, CH_2O is underestimated in both simulations, suggesting an underprediction of the chemical production of secondary CO. A similar effect to that described in Gaubert et al. (2016) is shown, where an increase in CO through the sequential assimilation leads to reduced OH and is slowing down the VOC oxidation rate and formaldehyde formation, albeit a small effect. In the lower part of the atmosphere, the oxidation of additional CO leads to more effective ozone production and no changes above, consistent with observations. While the errors in NO_x are important, the low CH_2O points to a missing source, which could be due to an underestimation of NMVOCs.

620

625
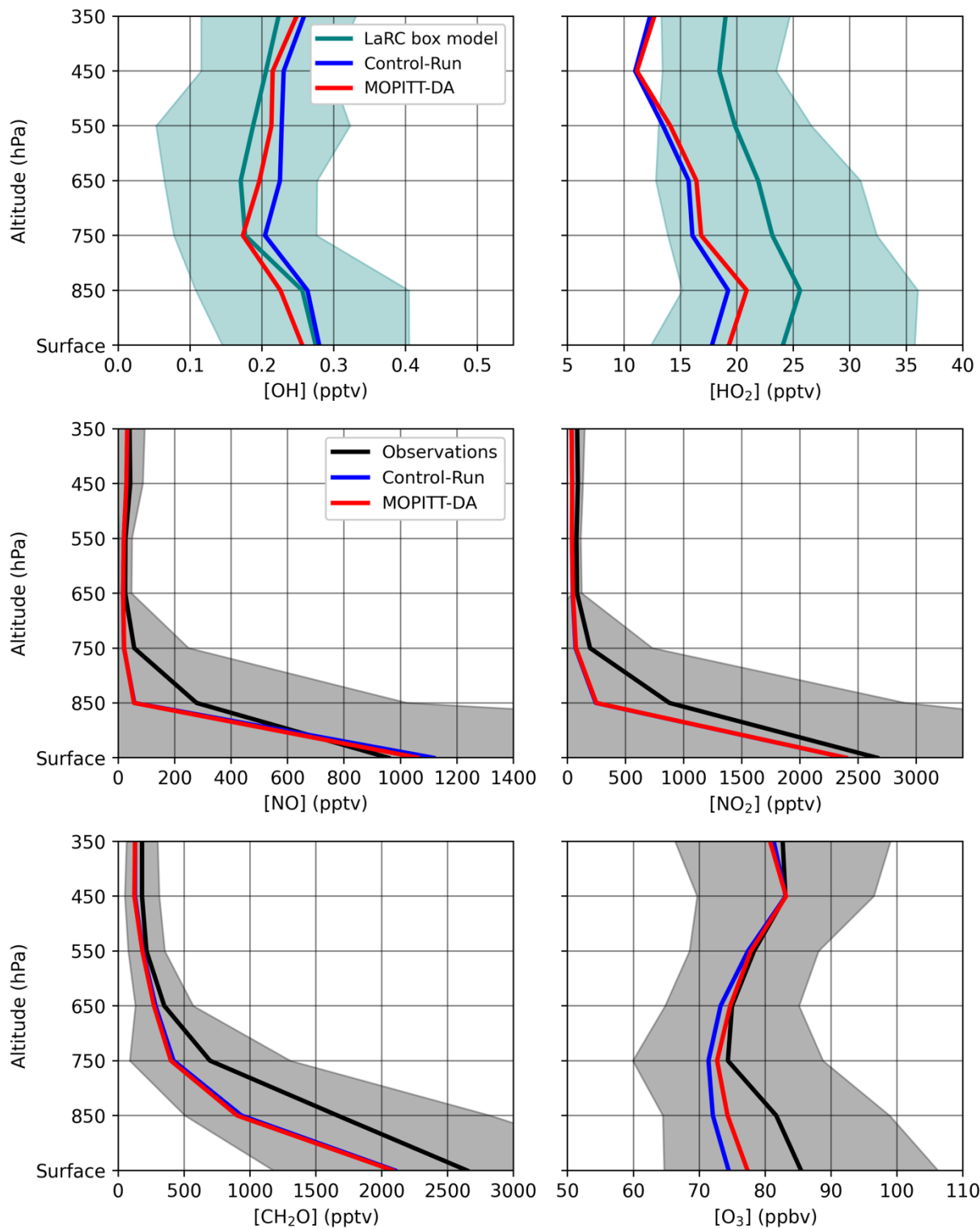
Figure 4: Average vertical profiles of OH (top left) HO₂ (top right) for the 1-sec merge and the LaRC box model estimates (Schroeder et al., 2020). Results are shown for DC-8 1-min merge observations for NO (middle left), NO₂ (middle right), CH₂O (bottom left) and O₃ measurements (bottom right). The shaded area corresponds to the standard-deviation around the observed mean.

630

6. Comparison of anthropogenic emission estimates

635   We show in Figure 5 the emissions of the prior (CEDS-KORUSv5), and its posterior, estimated through the DART/CAM-chem inversion. It also shows the prior (HTAP v2) from the TCR-2 and its posterior estimate, for which CO emissions are also constrained by MOPITT. We also show the CAMS emissions.
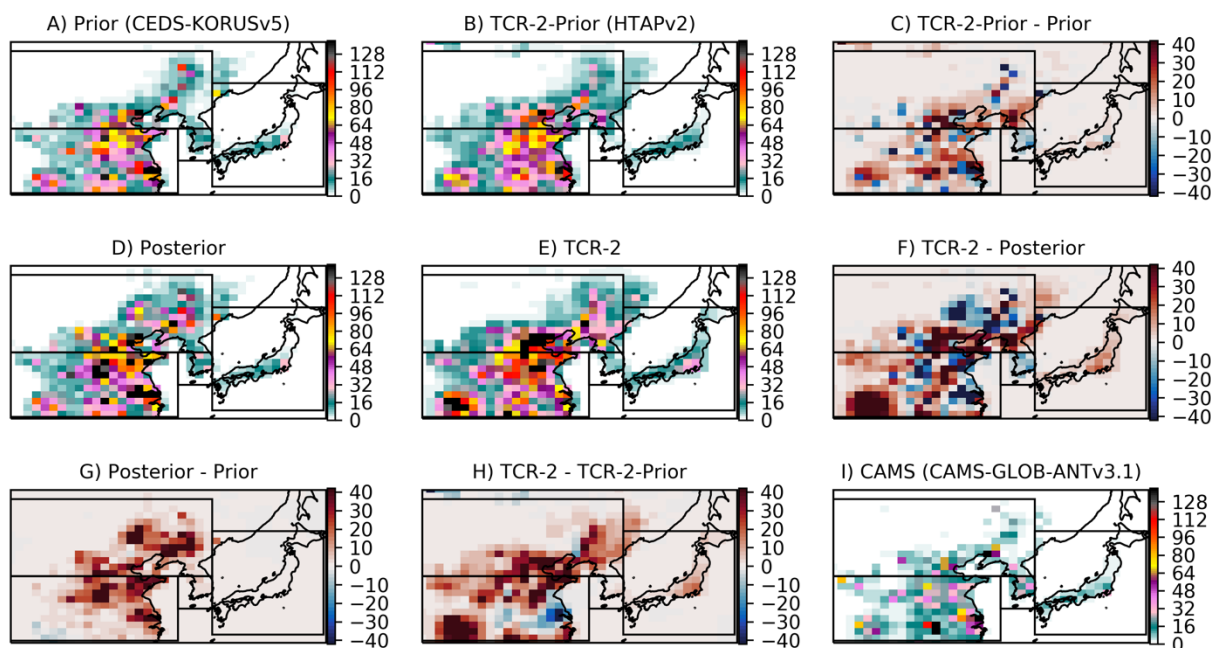
640

Figure 5: Emissions flux for May 2016 in MgCO.month^{-1}. Prior (A, CEDS-KORUS v5), TCR-2-Prior (B, HTAP v2) and the difference between the 2 priors (C, TCR-2-Prior – Prior). The second row shows the Posterior (D, estimated by DART/CAM-Chem), the TCR-2 (E) and the difference between the 2 posteriors. The last row shows the emissions increments, the difference between the Posterior and the Prior (G) and between TCR-2

645   **and TCR-2-Prior (H). The CAMS emissions are shown on the last panel (I).**

Compared to the prior (Fig. 5a), our posterior estimate (Fig. 5d) shows a reduction around the Guizhou province, in southwest China. Larger changes are observed for the Shandong and Henan provinces in central China and over the Yangtze River Delta (Fig. 5g). Increases in emissions are

650   also large in the NCP and the Liaoning Province. While both inversions show large increase over northern China (Fig. 5g, h), the spatial patterns of the emissions are different between the posterior and the TCR-2 for northern China. The TCR-2 emission increments are located more in the NCP and North Korea (Fig. 5f). Large differences can be identified in central China in particular over the YRD (Fig. 5h. The Shanghai megacity emissions are higher in the DART/CAM-chem posterior

655   (Fig. 5d) and the TCR-2 prior (Fig. 5b) than in the TCR-2 posterior (Fig. 5e). A more consistent pattern of larger emissions in the TCR-2 compared to our posterior is found in southern China and the Sichuan province (Fig. 5f and Fig. 5h). Prior emissions of CO, biogenic and anthropogenic VOCs and NOx can all contribute to differences between the TCR-2 and our DART/CAM-chem estimate. Another important aspect is the 500 km correlation length initial perturbation to generate

660   the ensemble of anthropogenic emissions, combined with a similar localization radius of ~600 km, which explains the large-scale increments found in the DART/CAM-chem emissions increments (Fig 5g). The TCR-2 prior show more emissions over North Korea than South Korea (Fig 5b) and the opposite is true for the DART/CAM-Chem prior (Fig 6c). This is reflected in the posterior where the TCR-2 has more emissions in North Korea than the DART/CAM-Chem posterior (Fig.

665   5f). Compared to its prior, the DART/CAM-Chem posterior emissions are increased by 25 % for South Korea, and by 34 % over the SMA. While the CAMS emissions are generally lower (Fig. 5i), the South Korean emissions are larger than in all the other inventories.

670   Our inversion suggests an underestimation of bottom-up emission inventories for China. The agreement between the posterior emissions for Central China is better than for the bottom-up inventory (Fig. 6). The difference between CAMS (3.65 $TgCO.Month^{-1}$) and the CEDS-KORUSv5 (5.7 $TgCO.Month^{-1}$) is twice as high as the difference between DART/CAM-chem posterior (7.6 $TgCO.Month^{-1}$) and TCR-2 (8.7 $TgCO.Month^{-1}$). On average, the increase in emissions due to assimilation is about 33 % for central China and nearly doubled (80 %) in Northern China, from
675   2.7 $TgCO.Month^{-1}$ to 4.9 $TgCO.Month^{-1}$. TCR-2 suggests higher emissions (5.7 $TgCO.Month^{-1}$), while the CAMS estimate is lower (1.8 $TgCO.Month^{-1}$). More work should be dedicated to check whether the assumptions made on the prior estimates impact the retrieved emissions. This includes improving the regional distribution and scaling up the baseline prior CO emissions, but also how much the model uncertainties in the OH chemical sink impact the CO inversions (e.g., Müller et
680   al., 2018). A comparison of the amount of residential coal burning emissions in bottom-up inventories could help in understanding the discrepancy and quantifying potential offsets (Chen et al., 2017; Cheng M., et al., 2017; Zhi et al., 2017, Benish et al., 2020).

685   For South Korea, a relatively smaller difference between the posterior and the prior suggests an improved bottom-up inventory. However, the smaller area of South Korea is much less constrained by MOPITT, and the overall estimate seems to be determined by the prior distribution. For instance, the TCR-2 shows larger emissions over North Korea and the Pyongyang area while DART/CAM-chem and CAMS suggests larger emissions for the SMA. Therefore, the CAMS total emissions that show a similar pattern (0.18 $TgCO.Month^{-1}$) are in good agreement with the
690   DART/CAM-chem (0.16 $TgCO.Month^{-1}$) while the TCR-2 has a total of 0.07 $TgCO.Month^{-1}$. For Japan, where biomass burning and low-tech coal combustion are rare, the total is nearly unchanged in contrast to the other regions, and emissions are increased from 0.38 to 0.41 $TgCO.Month^{-1}$ or 8 %.
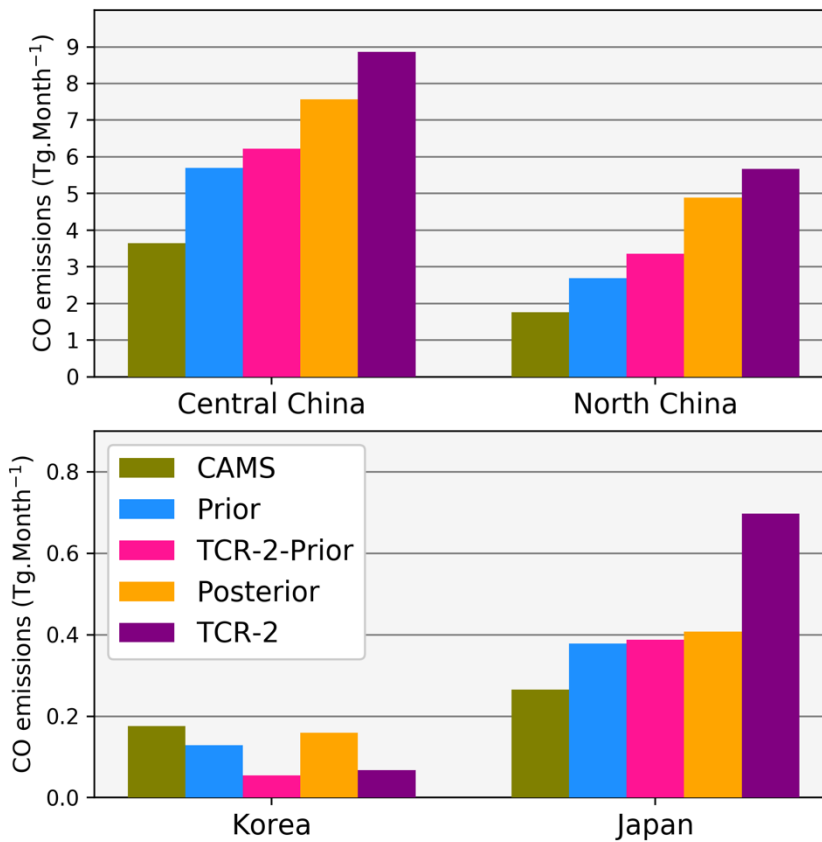
Figure 6: Anthropogenic CO emissions for May 2016 for Central China (91E, 29N to 124E, 38N), North China (91E, 38N to 130E, 49N), South Korea (125E, 33.5N to 129E, 38N) and Japan (130E, 30N to 146E, 44N).

7. Evaluation of the simulated vertical profiles against ARIAs and KORUS-AQ

This section presents the evaluation of the simulated profiles of CO, O_3, OH, and HO_2 with the observations from ARIAs and KORUS-AQ.

7.1 Mean profile during ARIAs and KORUS-AQ

Figure 7 shows the average CO vertical profiles for the ARIAs and the KORUS-AQ campaigns. For the ARIAs field campaign, we bin the profiles into 50 hPa bins. Overall, CO observations show a strong variability, with large enhancement over a background of around 170 ppbv found at 775 hPa and above. Benish et al. (2020) show that the median of the observed CO values in the lowest 500 meters is around 400 ppbv. Using additional enhancement ratios, the measurements indicate low-efficiency fossil fuel combustion, that could originate from residential coal burning and gasoline vehicles as well as crop residue burning such as straw from winter wheat. The MOPITT-DA and the TCR-2 overestimate the CO concentrations compared to the measurements for this surface layer although this overestimate is smaller by 60 % for TCR-2 and by 30 % for MOPITT-DA when a value higher than 20 ppbv SO_2 (the approximate 95th percentile) is used to define plumes for exclusion. The CAM-chem posterior simulated CO concentrations, that just use the smoothed posterior emissions from the MOPITT-DA have a mean value closer to the observations. While both simulations do not have exactly the same transport, the remaining underestimation is likely to be due to the sequential data assimilation in the MOPITT-DA runs that

compensate for the remaining biases. Interestingly, the HTAP v2 inventory that was for the year 2010 still provides good CO profiles (CAM_HTAP). The CAM_Kv5, a nudged CAM-chem simulation, and the Control-Run, underestimate CO concentration, with slight differences due to transport. The modeled profile with CAMS emissions profiles is the lowest CO of all simulations.

For altitudes ranging between 900 hPa and 600 hPa, the bias is lowest using the TCR-2 emissions or with the MOPITT-DA, because these emissions are more spatially representative of regional pollution (Wang et al., 2018). This confirms that the free-tropospheric background is too low in CAM_Kv5 and CAM-CAMS. The MOPITT-DA naturally shows the lowest bias in CO concentrations in the free troposphere. The 875 hPa (900 to 850 hPa) layer mean (and median) observed ozone during ARIAs (Benish et al., 2020) is around 80 to 90 ppbv and the mean peaks at 90 ppbv. For this layer, higher O_3 was found for simulations with higher CO. While it suggests that reducing CO biases can improve O_3, NO_2 and NMVOCs such as aromatics seem to play an important role in the ozone formation in the region (Benish et al., 2020). The mean O_3 concentration is still underestimated by around 10 ppbv in the free troposphere.
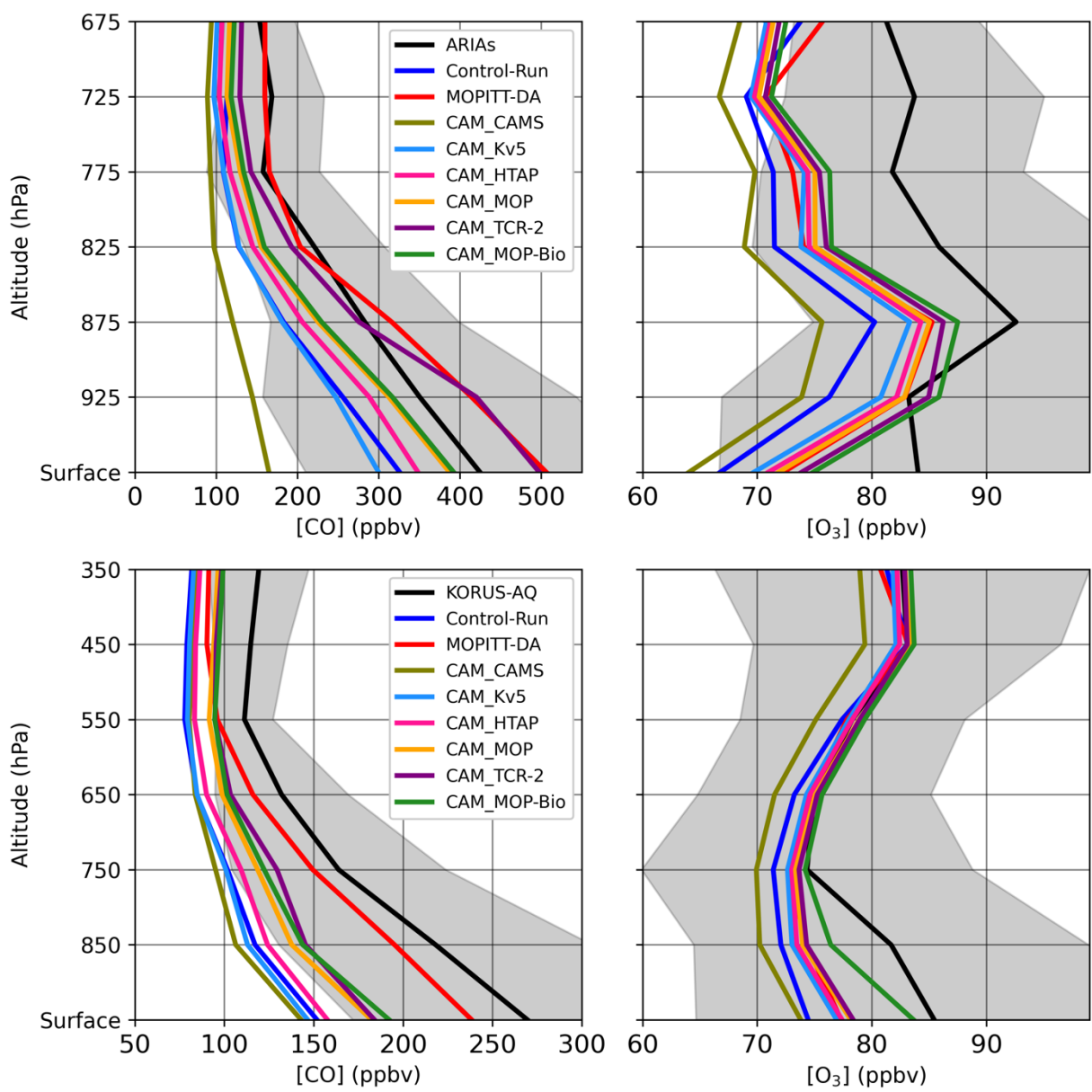
735 Two groups appear when comparing to KORUS-AQ observations. The Control-Run and CAM_Kv5, using CEDS-KORUS v5 with two different model dynamics and CAM_CAMS are simulating a lower CO and show a severe low bias of more than 100 ppbv at the surface. The second group includes the CAM-chem simulations using posterior emission estimates. Those simulations are quite close together with an average for all altitude layers of CO of 141 ppbv and

740 145 ppbv with a bias of 31 % and 29 % respectively (Table 4). This is to be compared with their priors that have an average CO of 116 ppbv and 125 ppbv, which implies an underestimation of 43 % and 39 %, respectively. Correcting only the bias in anthropogenic emissions is not as efficient as the joint optimization of anthropogenic emissions and sequential optimization of initial conditions through data assimilation (MOPITT-DA). It suggests that other sources of errors such

745 as transport and chemistry can be mitigated by state assimilation. The MOPITT-DA has an average CO of 179 ppbv, resulting in 12 % underestimation on average (Table 4), which is well between the range in measurement and representativeness errors. Aside from CAM_CAMS, the modeled free tropospheric O3 shows no particular bias. The enhancement of observed O3 closer to the surface is underestimated in all simulations. The optimized emissions lead to an increase of a few

750 ppb in O3, bringing those simulations closer to the observations. In summary, using top-down estimates of CO emissions clearly improves the CO and O3 vertical profiles against independent observations over China and Korea.

755 **Table 4: Comparison of CO (ppbv) measured aboard the DC-8 and model simulation for all altitudes. Statistical indicators are calculated for phase 1 (7 flight days, 2952 observations), phase 2 (4 flight days, 2029 observations), phase 3 (3 flight days, 1243 observations), phase 4 (5 flight days, 2448 observations) and the whole campaign (20 flight days, 9099 observations).**

	CO (1)	Bias (%)	CO (2)	Bias (%)	CO (3)	Bias (%)	CO (4)	Bias (%)	CO (All)	Bias (%)
Observation	173.1		198.3		246.8		211.2		203.6	
Control-Run	114.5	-33.8	108.6	-45.2	138.7	-43.8	115.3	-45.4	118.6	-41.8
MOPITT-DA	146.5	-15.4	168.3	-15.1	230.6	-6.6	182.8	-13.5	178.5	-12.4
CAM_CAMS	108.1	-37.6	110.4	-44.3	112.2	-54.5	119	-43.6	112.8	-44.6
CAM_Kv5	112.3	-35.1	110.8	-44.1	124.7	-49.5	115.7	-45.2	115.9	-43.1
CAM_HTAP	118.7	-31.4	115.3	-41.8	137.3	-44.4	128.5	-39.2	124.6	-38.8
CAM_MOP	136	-21.4	131.8	-33.5	157.1	-36.3	139.5	-33.9	140.9	-30.8
CAM_TCR-2	138.4	-20	128.9	-35	174.4	-29.3	146.1	-30.8	145	-28.8
CAM_MOP-Bio	138.4	-20.1	137.2	-30.8	163	-34	151.8	-28.1	147.2	-27.7

760 ## 7.2 Weather induced dynamical change in CO during KORUS-AQ

Figure 8 shows the CO anomalies during KORUS-AQ for the observations and the simulations. The CO anomalies are largest in phase 3, with an enhancement of almost 100 ppb at 850 hPa. This transport phase, defined and described in Peterson et al. (2019) was characterized by high levels of ozone (>60 ppbv) and PM₂₅ (>50 µg/m³) because of efficient transport of low-level pollution

765 (Huang et al., 2018; Miyazaki et al., 2019; Choi et al., 2019). The model reasonably reproduced the variability of the different phases, albeit with insufficient magnitude. The desired magnitude is only achieved when including data assimilation. Updating the anthropogenic emissions from the bottom-up to the top-down inventories improved the representation of the CO anomalies. This suggests that weather patterns and the direct anthropogenic emissions explain some of the CO
770 variability during the campaign. However, since only the MOPITT-DA simulation is reproducing well the anomalies, it suggests that chemistry and transport are important too. Large-scale subsidence and reduced wind speeds during the anticyclone of phase 2 were marked by the lowest CO anomalies and are also better reproduced with the updated emissions. Over South Korea, running CAM-chem with the CAMS emissions shows the largest anthropogenic CO from South
775 Korean sources at the surface for the 4 phases and is likely to produce more realistic simulation since CO is constantly underestimated. This cannot be seen for the total CO since most of the CO is not from South Korean direct anthropogenic sources. The profile tags of the contributions from Central China and Northern China are approximately doubled with the optimized emissions, consistent with Tang et al. (2019). As shown in the previous section, the CAM_TCR-2 and the
780 DART/CAM-chem posteriors have the largest emissions from China and therefore the largest contribution of the CO tags from both Northern and Central China.
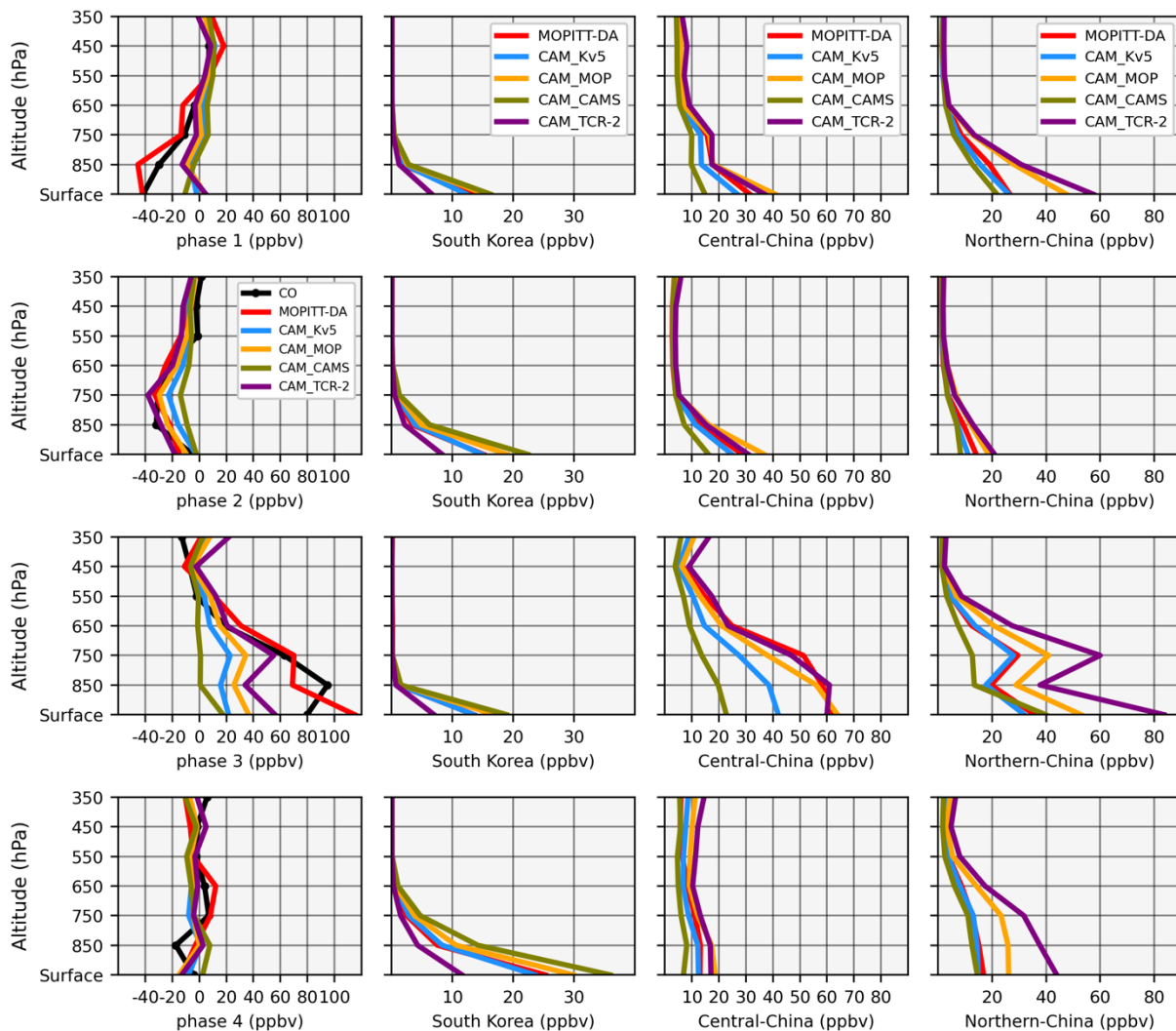
Figure 8: Average CO anomalies for the four different phases of KORUS-AQ (first column). The anomaly is
785 **defined by subtracting the respective average vertical profile (see Fig. 2). Absolute vertical profiles of the CO**

We will now focus on two case studies, Phase 2 and Phase 3, for which the highest ozone was
790   observed at the surface in South Korea during KORUS-AQ (Peterson et al., 2019).

7.3 Phase 2 case study: the anticyclonic phase

A large-scale anticyclone occurred from 17 May 2016 to 22 May 2016 with increased surface temperatures, reduced wind speed and drier conditions, all of which enhance ozone production (Peterson et al., 2019). The conditions were also favorable to an increase in biogenic emissions.
795   As shown in the previous sections, this episode was characterized by negative CO anomalies that were best captured by the MOPITT-DA simulations. This anomaly is reflected through lower OH and higher O_3 between 800 hPa and 400 hPa (Figure 9). This indicates rather clean air masses, probably with larger stratospheric contribution. This episode is driven by the overall weather pattern with a clear enhancement of HO_x and O_3 towards the surface. In this case, changes in the
800   anthropogenic CO only play a minor role, still the O_3 is modeled better with a reduction of the bias by 1 ppbv between the posterior and the prior (Table 5). The increase in biogenic emissions leads to an improvement in O_3 by further reducing the bias at the surface (Figure 9). Over the whole profile, the bias is reduced by 3 ppbv (4 ppbv against the prior) for the CAM_MOP-Bio, compared to the CAM_MOP, with a reduction in RMSE as well (Table 5).
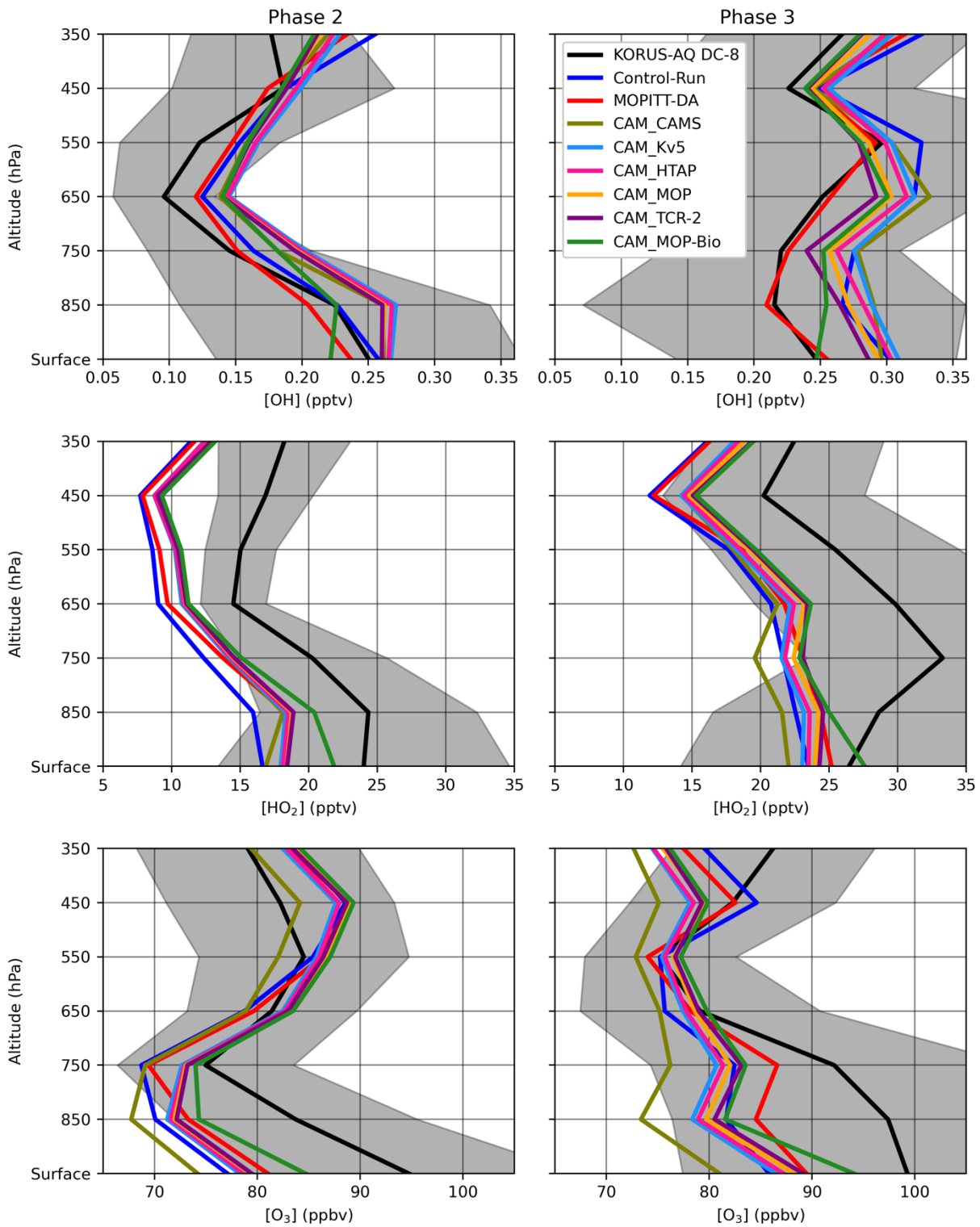
805

Figure 9: Average LaRC box model OH and HO₂ and measured O₃ for phase 2 (left column) and phase 3 (right column) of KORUS-AQ.

7.4 Phase 3 case study: low-level transport and haze development.

810   Phase 3 was characterized by the largest observed CO and O_3 positive anomalies. In this case, there is a clear relationship between the CO bias, and the O_3, OH and HO_2 vertical profiles (Figure 9).

The OH is overestimated because of a lack of CO, other VOCs and errors in the vertical profile of NO_x. Increasing CO in the CAM_MOP reduces OH and increases HO_2 and O_3. The overall bias (Table 5) in ozone is reduced from 11.3 ppbv to 9.9 ppbv with the change in CO, and lowered further to 7.3 ppbv with the additional increase in biogenic emissions (CAM_MOP-Bio). The relative impacts of biogenics are clear in the surface layer for OH, HO_2 and O_3. Overall, HO_2 and O_3 are underestimated as a result of CO underestimation. The MOPITT assimilation provides the best results for OH throughout the profile and lower RMSE and a similar bias as the CAM_MOP-Bio (Table 5). As suggested by the Chinese origin of the pollution for higher levels, it is likely that additional anthropogenic NMVOCs are also missing and contribute to the ozone formation that is still underestimated.

Table 5: Comparison of O_3 measured aboard the DC-8 and model simulation for all altitudes. Statistical indicators are calculated for phase 2 (4 flight days, 1910 observations), phase 3 (3 flight days 1111 observations) and all KORUS-AQ.

	O_3 (Phase 2)	Bias	RMSE	O_3 (Phase 3)	Bias	RMSE	O_3 (All)	Bias	RMSE
Observation	87.7			91.5			82.1		
Control-Run	77.2	-10.6	19.6	81.8	-9.7	20.4	75.1	-7	16.8
MOPITT-DA	79.7	-8	18.1	83.8	-7.7	19.5	76.9	-5.2	15.9
CAM_CAMS	74.4	-13.3	20.7	76.1	-15.4	24.2	73.6	-8.5	18.8
CAM_Kv5	78.2	-9.6	18.5	80.2	-11.3	21.5	76.5	-5.6	17.4
CAM_HTAP	78.5	-9.2	18.4	80.7	-10.8	21.2	76.9	-5.2	17.3
CAM_MOP	79.1	-8.6	18.2	81.6	-9.9	20.8	77.6	-4.5	17.2
CAM_TCR-2	79.2	-8.6	18.1	82.2	-9.2	20.5	77.8	-4.4	17.1
CAM_MOP-Bio	82.3	-5.5	15.9	84.2	-7.3	20.2	80.5	-1.6	16.5

8 Conclusions

Anthropogenic CO emissions are an important contributor to poor summer air quality in Asia and to forward modelling uncertainties. Here we evaluate top-down estimates of the CO emissions in East Asia with aircraft observations from two extensive field campaigns. There are multiple lines of evidence that the bottom-up anthropogenic emissions are too low in winter and spring, leading to a large underestimation of CO during the KORUS-AQ campaign in May and June 2016. We also highlight in this work that chemical production and loss via OH reaction from emissions of anthropogenic and biogenic VOCs confound the attribution of this bias in current model simulations. Combined initial conditions and emission optimization remains the best method to overcome these modeling issues. The major findings of this investigation are:

1. The comparison of OH modeling and observations confirms that assimilating CO improves the OH chemistry by correcting the OH/HO_2 partitioning. The interactive and moderately comprehensive chemistry with resolved weather from reanalysis datasets represents well the variations in OH. These results provide an additional line of evidence that assimilating CO improves the representation of OH in global chemical-transport models. This has implications for studying the CH_4-CO-OH coupled reactions and the impact of chemistry and interactive chemistry for allowing feedbacks. It suggests that even if global mean OH is buffered on the global scale, local changes in OH can be important, and can be quantified by taking advantage of field campaigns. This will provide ways to improve and provide additional constrain on CH_4 inversions by either improving the sink or by better

characterizing anthropogenic sources through CO assimilations. A better quantification of the spatio-temporal variability of these compounds will improve the physical representation of Earth system processes and feedbacks and will be beneficial for both air quality and climate change mitigation scenarios.

850

2. The setup of the CO assimilation that corrects the initial conditions and emissions provides the best results for CO. While the emission update improves the forecast closer to the source, the assimilation allows for better reproduction of the vertical profiles and the background and eventually compensates for model errors.

855

3. The spread of emission estimates from state-of-the-art inventories, 3 bottom-up and 2 top-down is significant. For example, the emissions of Central China show a range from 3.65 $TgCO.month^{-1}$ to 8.87 $TgCO.month^{-1}$. Inventories with the highest emissions fluxes show improved vertical profiles of CO.

4. Running the forward model with updated emissions of anthropogenic CO increases the O_3

860

formation, reduces OH and increases HO_2. This improves the comparison with O_3, OH and HO_2 observations. The comparison with observations suggests that the overall modeled photochemistry was improved with updated CO emissions. In this case, there is also a better representation of severe pollution episodes with large O_3 values. Often overlooked, it clearly shows that running chemistry transport models with biased CO and VOCs

865

emissions results in poorly modeled ozone and impacts most of the chemical state of the atmosphere. The sensitivities may vary for different chemical and physical atmospheric environments. In this case, underestimating CO in VOC-limited chemical regimes explains the underestimation of ozone in the boundary layer and the lower free troposphere.

5. Biogenic emissions appear to play an important role in ozone formation over South Korea,

870

in particular when conditions are favorable (sunny and warm). The role is weaker over China, at least in May before maximum biogenic emission rates. A combined assimilation of CO and CH_2O observations is likely to greatly improve ozone forecasting through estimates of boundary and initial condition estimates of VOCs.

875

On top of CO data assimilation, improved emissions through state augmentation can help improve the next-generation of Korean (e.g., Lee et al. 2020) or global (Barré et al., 2019) air quality analysis and forecasting systems. Further improvements can be achieved by simultaneously assimilating CH_2O retrievals (e.g. Souri et al., 2020) and CO retrievals. Improving the aerosol distribution can help correct the HO_2 uptake and therefore OH, CO and O_3 by assimilating satellite

880

aerosol optical depth measurements, in particular for this region with high aerosol loadings (e.g. Ha et al., 2020). Using CrIS-TROPOMI joint retrievals (Fu et al. 2016), the improved vertical sensitivity may potentially be used to further constrain secondary CO formed through biogenic oxidation. In this case, secondary CO is correlated with ozone formation. This is also true for other geographical areas, such as over the United States in summer (Cheng et al., 2017, 2018). On

885

average, there is a lower combustion efficiency in China than in Korea, with the ratio of CO to CO_2 changing accordingly as shown by the DC-8 measurements during KORUS-AQ (Halliday et al., 2019) and indicated by model simulations (Tang et al., 2018). Tracking CO_2 and CO from fossil fuel emissions could be combined to further constrain fossil fuel emission fluxes.

890

Many studies have focused on the long-term CO emission trends now well characterized (Zheng et al., 2019). For the sake of forward modeling (see e.g. Huang et al., 2018), it is important to focus on improving the absolute emission totals and their spatio-temporal distribution. While bottom-up inventories are critical, the next step is a comparison of inverse modelling estimates in combination with aircraft observations (e.g. Gaubert et al., 2019) to assess transport, chemistry and deposition

895

error. Multi-model estimates of the emissions will provide improved error bars on the CO budget,

and hopefully reduced uncertainties from chemistry and meteorology (e.g. Müller et al., 2018; Miyazaki et al., 2020a).

Appendix A: KORUS-AQ DC-8 instrumentation

CO and CH_4 were both measured using the fast-response (1 Hz), high-precision (0.1 % for CH_4, 1 % for CO) and high accuracy (2 %) NASA Langley Differential Absorption CO Measurement or DACOM (Sachse et al. 1987). Based on the differential absorption technique, CO and CH_4 were measured using an infrared tunable diode laser. The instrument has been used in many field campaigns and has been useful to evaluate profiles retrieved from satellite remote sensing of CO (Warner et al., 2010; Tang et al., 2020). Formaldehyde was measured using the Compact Atmospheric Multispecies Spectrometer (CAMS), also at 1 Hz (Richter et al., 2015). NO, NO_2 and O_3 were measured by the NCAR chemiluminescence instrument (Ridley and Grahek 1990; Weinheimer et al., 1993). Nitric acid (HNO_3), hydrogen peroxide (H_2O_2) and methyl hydroperoxide (CH_3OOH) were measured using the California Institute of Technology Chemical Ionization Mass Spectrometer (CIT-CIMS) (Crounse et al., 2006). Among the 82 speciated VOCs sampled by the discrete Whole Air Sampling (WAS) followed by multi-column gas chromatography (Simpson et al., 2020), we used ethyne (C_2H_2), ethane (C_2H_6), ethene (C_2H_4) and propane (C_3H_8). All the larger alkanes (i-butane, n-butane, i-pentane, n-pentane, n-hexane, n-heptane, n-octane, n-nonane, n-decane), alkenes (1-butene, i-butene, trans-3-butene and 1-3-butadiene) and xylenes (mp-xylene, o-xylene) were summed (Table 3) for the comparison with the BIGALK, BIGENE and XYLENES respectively of the T1 surrogate species (Emmons et al., 2020). Methanol (CH_3OH), acetaldehyde (CH_3CHO), acetone (CH_3COCH_3), benzene (C_6H_6) and toluene (C_7H_8) were measured with the proton-transfer-reaction time-of-flight mass spectrometer (PTR-ToF-MS) at 10 Hz frequency (Müller et al., 2014). We also evaluate some meteorological parameters, such as temperature and wind speed as well as water vapor moist volumetric mixing ratio measured by NASA open-path diode laser hygrometer (Podolske et al., 2003), with a 5% uncertainty. J values were measured using the CAFS instrument (Charged-coupled device Actinic Flux Spectroradiometer; Shetter and Müller, 1999; Petropavlovskikh et al., 2007).

Appendix B: CAM-chem updates

B1 CH_4 emissions from the Global Carbon Project CH_4

Radiatively active species, such as CH_4, are prescribed in CAM-chem using a latitudinal-monthly surface field derived from observations in the past and projections for the future, defined in the CMIP6 protocol (Meinshausen et al., 2017). In order to include the feedbacks in the CH_4-CO-OH chemical mechanism, we choose to apply CH_4 emissions instead of the prescribed field. The scope of the paper is not to study the methane budget; the objectives are to see how much CO is produced from CH_4 during the campaign. The long-term goal is to get sensitivities to changes according to CO emission updates in order to analyze the feedbacks on CH_4 when CO is changed. We used emissions from some of the inversions of a recent compilation of CH_4 budget from top-down estimates (Saunois et al., 2020). As a first step, we used the mean of the 11 inversions (Table B1) that assimilate CH_4 retrievals from the JAXA satellite Greenhouse Gases Observing SATellite (GOSAT, Kuze et al., 2009).

Table B1: List of the 11 methane inversions from the Global Methane Budget (Saunois et al., 2020), as indicated by the number of inversions column. All the details are presented in the references.

Institution / Model	Observation Used	Number of inversions	References
FMI / CarbonTracker Europe-CH$_4$	GOSAT NIES L2 v2.72	1	Tsuruta et al. (2017)
LSCE & CEA / LMDz-PYVAR	GOSAT Leicester V7.2	2	Yin et al. (2015)
LSCE & CEA / LMDz-PYVAR	GOSAT Leicester V7.2	4	Yin et al., (2019)
NIES / NIES-TMFLEXPART (NTFVAR)	GOSAT NIES L2 v2.72	1	Maksyutov et al. (2020); Wang et al. (2019)
TNO & VU / TM5-CAMS	GOSAT ESA/CCI v2.3.88 (combined with surface observations)	1	Segers (2020 report); Bergamaschi et al. (2010; 2013); Pandey et al., (2016)
EC-JRC / TM5-4Dvar	GOSAT OCPR v7.2 (combined with surface observations)	2	Bergamaschi et al., (2013, 2018)

B2 The HO$_2$ uptake by aerosol particles

The TS1 chemistry includes an HO$_2$ uptake by aerosol particles following the recommendation of Jaeglé et al. (2000) and Jacob et al. (2000), that form H$_2$O$_2$, with a reactive uptake coefficient γ of 0.2, as follow:

$$HO_2 + aerosols \rightarrow 0.5 * H_2O_2 \qquad \text{with } \gamma=0.2 \qquad\qquad (B1)$$
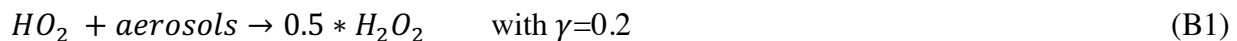
Based on Observations from the NASA Arctic Research of the Composition of the Troposphere from Aircraft and Satellites (ARCTAS) and other field campaigns, Mao et al. (2010, 2013) suggested a catalytic mechanism with transition metal ions (Cu and Fe) that rapidly converts HO$_2$ to H$_2$O instead of H$_2$O$_2$:

$$HO_2 + aerosols \rightarrow H_2O \qquad \text{with } \gamma=0.2 \qquad\qquad (B2)$$

Using Eq. B2 and γ=1 leads to a large loss of HOx, which in turn increases the CH4 and CO lifetime and thus reduces the CO bias during the high latitude winter (Mao et al., 2013). Christian et al. (2017) simulated a range of possible values of γ and evaluated the results against ARCTAS data and found that lower γ, closer to zero, gave a more realistic distribution of HO$_x$. Kanaya et al. (2009) studied ozone formation over Mount Tai, located in central East China, and looked at the possible influence of the heterogeneous loss of gaseous HO$_2$ radicals. They found that introducing the loss reduces HO$_2$ levels and increases ozone, with a more pronounced effect in the upper part of the boundary layer where the role of OH+NO2 +M reaction does not play a significant role in the radical termination reaction while the number density of aerosol particles is still important. Li

et al. (2018) found that the HO_2 uptake was the largest HOx sink in the upper boundary layer in northern China. They suggested that the reduction in HO_2 uptake caused by the decrease of aerosols was responsible for the increase of O_3 in the region. Thus, the initial comparison of CAM-chem using Eq. (B1) showed a large overestimation of H_2O_2. In a previous study using Eq. (B1), the increase in CO following data assimilation increased hydrogen peroxide (H_2O_2) levels (Gaubert et al., 2016). Therefore, it is expected that the hydrogen peroxide (H_2O_2) would be severely overestimated if Eq. (B1) is used. Miyazaki et al. (2019a) assimilated several satellite retrievals of chemical composition during KORUS-AQ, including MOPITT, and found a strong overestimation of H_2O_2 using Eq. (B1) in the chemical scheme of the MIROC-Chem model. Thus, the reaction in CAM-chem has been updated to Eq. (B2) with $\gamma=0.1$ prior to any data assimilation run.

B3 Results on HO_2 uptake and methane emissions

This section presents the results on the model update before the assimilation runs are conducted. Five CAM-Chem simulations were performed (Table B2), and CAM-Chem-Ref corresponds to the reference with prescribed CH_4 and Eq. (B2) for the HO_2 uptake. The CAM-H2O is performed with the update to Eq. 3 for the HO_2 uptake and the GCP-Ref is performed with the CH_4 emissions instead of the CH_4 prescribed field. The GCP-H2O contains the update on CH_4 emissions and on the HO_2 uptake and has been run with $\gamma=0.2$ and $\gamma=0.1$.

Table B2: description of the sensitivity test performed with CAM-Chem anterior to any assimilation run.

Simulation name	HO_2 uptake (γ)	Surface CH_4
CAM-chem-Ref	Eq. (2) ($\gamma=0.2$)	Prescribed
CAM-Chem-H2O	Eq. (3) ($\gamma=0.2$)	Prescribed
GCP-Ref	Eq. (2) ($\gamma=0.2$)	Emissions
GCP-H2O ($\gamma=0.2$)	Eq. (3) ($\gamma=0.2$)	Emissions
GCP-H2O ($\gamma=0.1$)	Eq. (3) ($\gamma=0.1$)	Emissions

Fig. B1 shows the average profiles for H_2O_2 and CH_4. There is a large bias in H_2O_2 for the reference simulation (CAM-chem-Ref) that is particularly large in the surface layer. The observed H_2O_2 at the surface is lower in the morning due to inhibited photochemical production and the nighttime deposition (Schroeder et al., 2020). Large model errors could then be due to uncertainties in the boundary layer height and wet deposition. However, this points to an underestimation of the H_2O_2 dry deposition, a common feature found due to an overestimation of surface resistance (Ganzeveld et al., 2006; Nguyen et al., 2015). The H_2O_2 daytime deposition velocities calculated at the location of the Taehwa Research Forest site ranged between 0.4 cm.s^{-1} and 1.3 cm.s^{-1}, which suggests an underestimation compared to the observed velocities of around 5 cm.s^{-1} reported in the literature (Hall and Claiborn, 1997; Hall et al., 1999; Valverde-Canossa et al. 2006; Nguyen et al., 2015). A simulation with a 5-fold increase of the H_2O_2 deposition velocity over land only partially reduces the H_2O_2 bias. Further work needs to be done to better understand the drivers of the H_2O_2 biases, which is beyond the scope of this study.

Interestingly, having CH_4 emissions (GCP-Ref) while keeping the original reaction (Eq. 2) gives a slightly better H_2O_2, suggesting that using optimized emissions instead of a prescribed concentration field has an effect on the oxidants' distribution. The three simulations with the updated chemistry out-perform the references with biases almost halved. This is particularly true for the free troposphere. The modeled H_2O_2 profile seems rather insensitive to the choice of the γ value. Since the simulations with the $\gamma=0.1$ performs slightly better, all following simulations will

be done with the updated reaction and γ=0.1. This is consistent with a recently published studies that diagnosed a median γ value of 0.1 over the NCP region (Song et al., 2020).

1010   Using emissions instead of fixed boundary conditions improves the simulated CH$_4$ near the surface, but with a lower tropospheric background (Figure A1). The comparison with CH$_4$ observations indicates a general underestimation. At this point, it is difficult to determine why it is underestimated.

1015   A first reason could be a too strong CH$_4$ sink in the model compared to the sink considered in the inversions that derived the GCP emissions. However, the prescribed CH$_4$ is not resolved in longitude, while the difference for a given latitude can be up to 300ppb when using emissions (see Fig S1). Emissions also have uncertainties and could be underestimated, or may have just been estimated with lower OH than the one CAM-chem simulates for this period. Saunois et al. (2020)
1020   showed that the GOSAT based inversions have lower emissions than the surface-based inversions for the northern mid-latitudes. It is likely that the errors observed during KORUS-AQ are a combination of both of those factors, as well as potential transport errors. Since the CH$_4$ profile is overall better reproduced with the GCP emissions, we have used the ensemble mean of the 11 GCP optimized emissions for the simulations presented in the main paper.

1025
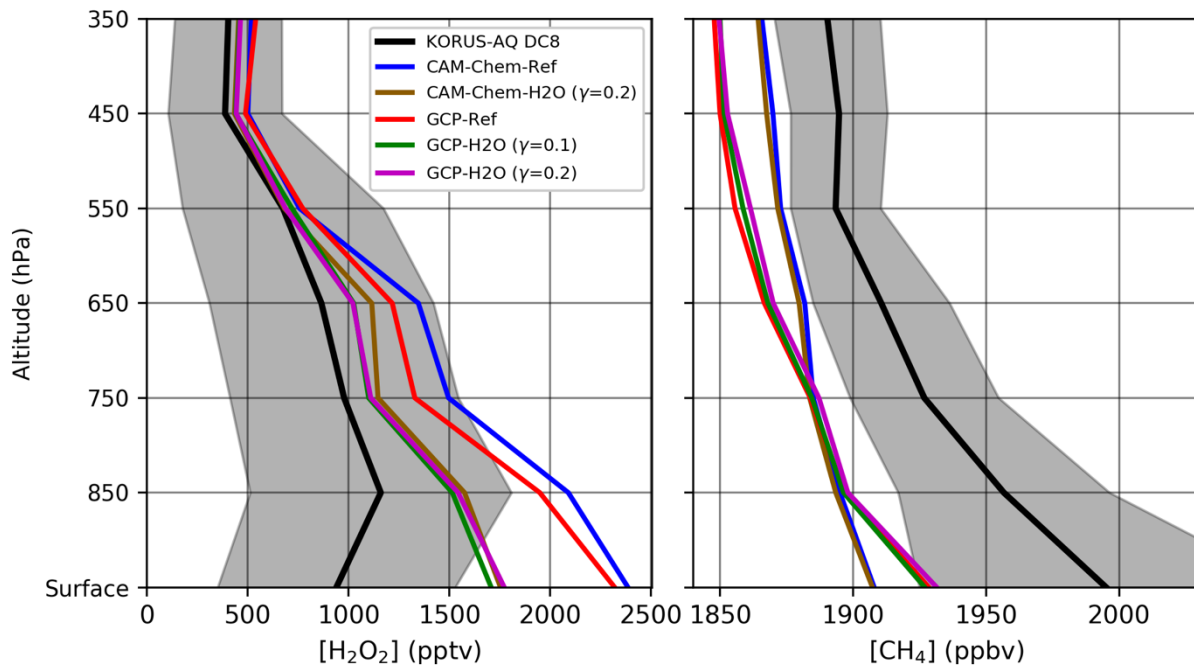
Figure B1: Average H$_2$O$_2$ profiles (left panel) and CH$_4$ profiles (right panels) for all KORUS-AQ. The mean (black line) and standard deviation (shaded grey) of the DC-8 observations are calculated for each 100 hPa bins and only the mean is shown for model simulations.

1030

Acknowledgments. We thank the editor Tim Butler and two anonymous reviewers for the constructive comments and useful suggestions. We would like to acknowledge high-performance computing support from Cheyenne (doi:10.5065/D6RX99HX) provided by NCAR's Computational and Information Systems Laboratory, sponsored by the National Science
1035   Foundation. Neither the European Commission nor ECMWF is responsible for any use that may

be made of the information it contains. We thank Yi Yin, Arjo Segers, Aki Tsuruta, Peter Bergamaschi, Bo Zheng for sharing their CH_4 inversions. We acknowledge James H. Crawford, Glenn S. Diskin, Alan Fried, Andrew Weinheimer and everybody that contributed to the KORUS-AQ campaign. The PTR-MS instrument team (P. Eichler, L. Kaser, T. Mikoviny, M. Müller, A.
1040 Wisthaler) is acknowledged for providing the PTR-MS data for this study. We also thanks Duseong Jo for reading the manuscript.

Financial support. This research has been supported by NASA (NNX16AD96G). This study was also supported by NOAA's Climate Program Office's Modeling, Analysis, Predictions, and
1045 Projections program (NA18OAR4310283). The NCAR MOPITT project is supported by the National Aeronautics and Space Administration (NASA) Earth Observing System (EOS) Program. Observations made by Caltech were sponsored by NASA (NNX15AT97G). This material is based upon work supported by the National Center for Atmospheric Research, which is a major facility sponsored by the National Science Foundation under cooperative agreement no. 1852977. The
1050 CESM project is supported primarily by the National Science Foundation (NSF). The ARIAs campaign was supported by the National Science Foundation (Grant # 1558259). Part of this work was conducted at the Jet Propulsion Laboratory, California Institute of Technology, under contract with the National Aeronautics and Space Administration (NASA). PTR-ToF-MS measurements aboard the NASA DC-8 during KORUS-AQ were supported by the Austrian Federal Ministry for
1055 Transport, Innovation and Technology (bmvit) through the Austrian Space Applications Programme (ASAP) of the Austrian Research Promotion Agency (FFG).

Code and datasets. CESM2.1.0 is a publicly released version of the Community Earth System Model and freely available online (at www.cesm.ucar.edu/, last access: 2 April 2020). The Data
1060 Assimilation Research Testbed is an open source software, code and documentation are available at https://dart.ucar.edu/ (DART, 2020). The Korea-United States Air Quality Field Study (KORUS-AQ) dataset is available at https://doi.org/10.5067/Suborbital/KORUSAQ/DATA01. The ARIAs observational dataset is available at https://www-air.larc.nasa.gov/missions/korus-aq/index.html. MOPITT data are available at https://www2.acom.ucar.edu/mopitt. The
1065 Tropospheric Chemistry Reanalysis version 2 is available for download at https://tes.jpl.nasa.gov/chemical-reanalysis/products/monthly-mean/. The Copernicus Atmosphere Monitoring Service (CAMS) global bottom-up emission inventory is available on the Emissions of atmospheric Compounds and Compilation of Ancillary Data (ECCAD) web site (https://eccad3.sedoo.fr).

1070

Competing interests. The authors declare that they have no conflict of interest.

References

Anderson, J. L.: An ensemble adjustment Kalman Filter for data assimilation, Mon. Weather Rev., 129, 2884–2903, https://doi.org/10.1175/1520-0493(2001)129<2884:AEAKFF>2.0.CO;2, 2001.

Anderson, J. L.: A local least squares framework for ensemble filtering, Mon. Weather Rev., 131, 634–642, https://doi.org/10.1175/1520-0493(2003)131<0634:ALLSFF>2.0.CO;2, 2003.

Anderson, J. L.: An adaptive covariance inflation error correction algorithm for ensemble filters, Tellus A, 59, 210–224, https://doi.org/10.1111/j.1600-0870.2006.00216.x, 2007.

Anderson, J. L., Hoar, T., Raeder, K., Liu, H., Collins, N., Torn, R., and Avellino, A.: The Data Assimilation Research Testbed: a community facility, B. Am. Meteorol. Soc., 90, 1283-1296, https://doi.org/10.1175/2009BAMS2618.1, 2009a.

Anderson, J. L.: Spatially and temporally varying adaptive covariance inflation for ensemble filters, Tellus A, 61, 72–83, https://doi.org/10.1111/j.1600-0870.2008.00361.x, 2009b.

Akimoto, H., et al.: Long-range transport of ozone in the East Asian Pacific rim region, J. Geophys. Res., 101(D1), 1999– 2010, doi:10.1029/95JD00025, 1996.

Arellano Jr., A. F., Kasibhatla, P. S., Giglio, L., van der Werf, G. R., and Randerson, J. T.: Top-down estimates of global CO sources using MOPITT measurements, Geophys. Res. Lett., 31, L01104, https://doi.org/10.1029/2003GL018609, 2004.

Arellano Jr., A. F. and Hess, P. G.: Sensitivity of top-down estimates of CO sources to GCTM transport, Geophys. Res. Lett., 31, L21807, https://doi.org/10.1029/2006GL027371, 2006.

Arellano Jr, A.F., Raeder, K., Anderson, J.L., Hess, P.G., Emmons, L.K., Edwards, D.P., Pfister, G.G., Campos, T.L. and Sachse G.W.: Evaluating model performance of an ensemble-based chemical data assimilation system during INTEX-B field mission. Atmospheric Chemistry and Physics, 7(21), pp.5695-5710, https://doi.org/10.5194/acp-7-5695-2007, 2007.

Arellano Jr., A. F., Hess, P. G., Edwards, D. P. and Baumgardner D.: Constraints on black carbon aerosol distribution from Measurements of Pollution in the Troposphere (MOPITT) CO, Geophys. Res. Lett., 37, L17801, https://doi.org/10.1029/2010GL044416, 2010.

Barré, J., Gaubert, B., Arellano, A.F., Worden, H.M., Edwards, D.P., Deeter, M.N., Anderson, J.L., Raeder, K., Collins, N., Tilmes, S. and Francis, G.: Assessing the impacts of assimilating IASI and MOPITT CO retrievals using CESM-CAM-chem and DART. Journal of Geophysical Research: Atmospheres, 120(19), pp.10-501, https://doi.org/10.1002/2015JD023467, 2015.

Barré, J., Massart S, Ades M, Jones L, and Engelen R.: Emission optimisations first attempt based on the Ensemble of Data Assimilation for atmospheric composition. European Centre for Medium-Range Weather Forecasts, https://doi.org/10.21957/4grkg5ga0, 2019.

Benish, S. E., He, H., Ren, X., Roberts, S. J., Salawitch, R. J., Li, Z., Wang, F., Wang, Y., Zhang, F., Shao, M., Lu, S., and Dickerson, R. R.: Measurement Report: Aircraft Observations of Ozone,

1120   Nitrogen Oxides, and Volatile Organic Compounds over Hebei Province, China, Atmos. Chem. Phys. Discuss., https://doi.org/10.5194/acp-2020-194, in review, 2020.

Bergamaschi, P., Krol, M., Meirink, J. F., Dentener, F., Segers, A., van Aardenne, J., Monni, S., Vermeulen, A. T., Schmidt, M., Ramonet, M., Yver C., Meinhardt, F., Nisbet, E.G., Fisher R. E.,
1125   O'Doherty, S., and Dlugokencky, E. J.: Inverse modeling of European CH4 emissions 2001-2006. Journal of Geophysical Research, 115(D22), D22309. https://doi.org/10.1029/2010JD014180, 2010.

Bergamaschi, P., Houweling, S., Segers, A., Krol, M., Frankenberg, C., Scheepmaker, R. A.,
1130   Dlugokencky, E., Wofsy, S. C., Kort, E. A., Sweeney, C., Schuck, T., Brenninkmeijer, C., Chen, H., Beck, V., and Gerbig, C.: Atmospheric CH4 in the first decade of the 21st century: Inverse modeling analysis using SCIAMACHY satellite retrievals and NOAA surface measurements, Journal of Geophysical Research: Atmospheres, 118, 7350-7369, https://doi.org/10.1002/jgrd.50480, 2013.
1135

Bergamaschi, P., Karstens, U., Manning, A. J., Saunois, M., Tsuruta, A., Berchet, A., Vermeulen, A. T., Arnold, T., Janssens-Maenhout, G., Hammer, S., Levin, I., Schmidt, M., Ramonet, M., Lopez, M., Lavric, J., Aalto, T., Chen, H., Feist, D. G., Gerbig, C., Haszpra, L., Hermansen, O., Manca, G., Moncrieff, J., Meinhardt, F., Necki, J., Galkowski, M., O'Doherty, S., Paramonova,
1140   N., Scheeren, H. A., Steinbacher, M., and Dlugokencky, E.: Inverse modelling of European CH4 emissions during 2006–2012 using different inverse models and reassessed atmospheric observations, Atmos. Chem. Phys., 18, 901-920, https://doi.org/10.5194/acp-18-901-2018, 2018.

Bogenschutz, P. A., Gettelman, A., Morrison, H., Larson, V. E., Craig, C., and Schanen, D. P.:
1145   Higher-order turbulence closure and its impact on climate simulations in the Community Atmosphere Model, J. Climate, 26, 9655–9676, https://doi.org/10.1175/JCLI-D-13-00075.1, 2013.

Borsdorff, T., aan de Brugh, J., Pandey, S., Hasekamp, O., Aben, I., Houweling, S., and Landgraf
1150   J.: Carbon monoxide air pollution on sub-city scales and along arterial roads detected by the Tropospheric Monitoring Instrument, Atmos. Chem. Phys., 19, 3579-3588, https://doi.org/10.5194/acp-19-3579-2019, 2019.

Butler, T., Lupascu, A., Coates, J., and Zhu, S.: TOAST 1.0: Tropospheric Ozone Attribution of
1155   Sources with Tagging for CESM 1.2.2, Geosci. Model Dev., 11, 2825–2840, https://doi.org/10.5194/gmd-11-2825-2018, 2018.

Colman, J. J., Swanson, A. L., Meinardi, S., Sive, B. C., Blake, D. R., and Rowland, F. S.: Description of the analysis of a wide range of volatile organic compounds in whole air samples
1160   collected during PEM-Tropics A and B, Anal. Chem., 73, 3723–3731, https://doi.org/10.1021/ac010027g, 2001.

Conrad, R.: Soil microorganisms as controllers of atmospheric trace gases (H2, CO, CH4, OCS, N2O, and NO), Microbiol. Rev., 60, 609–640, 1996.
1165

Coman, A., Foret, G., Beekmann, M., Eremenko, M., Dufour, G., Gaubert, B., Ung, A., Schmechtig, C., Flaud, J.-M., and Bergametti G.: Assimilation of IASI partial tropospheric

columns with an Ensemble Kalman Filter over Europe, Atmos. Chem. Phys., 12, 2513–2532, https://doi.org/10.5194/acp-12-2513-2012, 2012.

Cooper, O. R., et al.: A case study of transpacific warm conveyor belt transport: Influence of merging airstreams on trace gas import to North America, J. Geophys. Res., 109, D23S08, doi:10.1029/2003JD003624, 2004.

Chan, K. R., Dean-Day, J., Bowen, S. W., and Bui, T. P.: Turbulence measurements by the DC-8 meteorological measurement system, Geophys. Res. Lett., 25, 1355–1358, https://doi.org/10.1029/97GL03590, 1998.

Chen, S., Xu, L., Zhang, Y., Chen, B., Wang, X., Zhang, X., Zheng, M., Chen, J., Wang, W., Sun, Y., Fu, P., Wang, Z., and Li, W.: Direct observations of organic aerosols in common wintertime hazes in North China: insights into direct emissions from Chinese residential stoves, Atmos. Chem. Phys., 17, 1259–1270, https://doi.org/10.5194/acp-17-1259-2017, 2017.

Cheng, M., Zhi, G., Tang, W., Liu, S., Dang, H., Guo, Z., et al.: Air pollutant emission from the underestimated households' coal consumption source in China. Science of the Total Environment, 580, 641–650. https://doi.org/10.1016/j.scitotenv.2016.12.143, 2017.

Cheng, Y., Y. Wang, Y. Zhang, G. Chen, J. H. Crawford, M. M. Kleb, G. S. Diskin, and Weinheimer A. J.: Large biogenic contribution to boundary layer O3-CO regression slope in summer, Geophys. Res. Lett., 44, https://doi.org/10.1002/2017GL074405, 2017.

Cheng, Y., Wang, Y., Zhang, Y., Crawford, J. H., Diskin, G. S., Weinheimer, A. J., and Fried, A: Estimator of surface ozone using formaldehyde and carbon monoxide concentrations over the eastern United States in summer. Journal of Geophysical Research: Atmospheres, 123. https://doi.org/10.1029/2018JD028452, 2018.

Choi, J, Park, RJ, Lee, HM, Lee, S, Jo, DS, Jeong, JI, Henze, DK, Woo, JH, Ban, SJ, Lee, MD, Lim, CS, Park, MK, Shin, HJ, Cho, S, Peterson, D and Song, CK.: Impacts of local vs. trans-boundary emissions from different sectors on PM2.5 exposure in South Korea during the KORUS-AQ campaign. Atmospheric Environment 203: 196–205. DOI: https://doi.org/10.1016/j.atmosenv.2019.02.008, 2019.

Christian, K. E., Brune, W. H., and Mao, J.: Global sensitivity analysis of the GEOS-Chem chemical transport model: ozone and hydrogen oxides during ARCTAS (2008), Atmos. Chem. Phys., 17, 3769–3784, https://doi.org/10.5194/acp-17-3769-2017, 2017.

Crippa, M., Guizzardi, D., Muntean, M., Schaaf, E., Dentener, F., van Aardenne, J. A., Monni, S., Doering, U., Olivier, J. G. J., Pagliari, V., and Janssens-Maenhout, G.: Gridded emissions of air pollutants for the period 1970–2012 within EDGAR v4.3.2, Earth Syst. Sci. Data, 10, 1987–2013, https://doi.org/10.5194/essd-10-1987-2018, 2018.

Crounse, J. D., McKinney, K. A., Kwan, A. J., and Wennberg, P. O.: Measurement of gas-phase hydroperoxides by chemical ionization mass spectrometry, Anal. Chem., 78, 6726–6732, https://doi.org/10.1021/ac0604235, 2006.

Crutzen, P. J., L. E. Heidt, J. P. Krasnec, W. H. Pollack, and Seiler W.: Biomass burning as a source of atmospheric gases CO, H2, N2O, NO, CH3Cl, and COS, Nature, 282, 253-256, https://doi.org/10.1038/282253a0, 1979.

1220   Danabasoglu, G., Lamarque, J.-F., Bacmeister, J., Bailey, D. A., DuVivier, A. K., Edwards, J., et al.: The Community Earth System Model Version 2 (CESM2). Journal of Advances in Modeling Earth Systems, 12, e2019MS001916. https://doi.org/10.1029/2019MS001916, 2020.

The Data Assimilation Research Testbed (Version Manhattan). Boulder, Colorado:
1225   UCAR/NCAR/CISL/DAReS. http://doi.org/10.5065/D6WQ0202, 2020.

Ding, K., Liu, J., Ding, A., Liu, Q., Zhao, T. L., Shi, J., Han, Y., Wang, H., and Jiang F.: Uplifting of carbon monoxide from biomass burning and anthropogenic sources to the free troposphere in East Asia, Atmos. Chem. Phys., 15, 2843-2866, https://doi.org/10.5194/acp-15-2843-2015, 2015.
1230
Diskin, G. S., Podolske, J. R., Sachse, G. W., and Slate, T. A.: Open-path airborne tunable diode laser hygrometer, Proc. SPIE 4817, Diode Lasers and Applications in Atmospheric Sensing, https://doi.org/10.1117/12.453736, 2002.

1235   Deeter, M. N., Edwards, D. P., Francis, G. L., Gille, J. C., Mao, D., Martínez-Alonso, S., Worden, H. M., Ziskin, D., and Andreae, M. O.: Radiance-based retrieval bias mitigation for the MOPITT instrument: the version 8 product, Atmos. Meas. Tech., 12, 4561–4580, https://doi.org/10.5194/amt-12-4561-2019, 2019.

1240   Edwards, D.P., Emmons, L.K., Hauglustaine, D.A., Chu, D.A., Gille, J.C., Kaufman, Y.J., Pétron, G., Yurganov, L.N., Giglio, L., Deeter, M.N. and Yudin V.: Observations of carbon monoxide and aerosols from the Terra satellite: Northern Hemisphere variability. Journal of Geophysical Research: Atmospheres, 109, D24, https://doi.org/10.1029/2004JD004727, 2004.

1245   Edwards, D.P., Emmons, L.K., Gille, J.C., Chu, A., Attié, J.L., Giglio, L., Wood, S.W., Haywood, J., Deeter, M.N., Massie, S.T. and Ziskin, D.C.: Satellite-observed pollution from Southern Hemisphere biomass burning. Journal of Geophysical Research: Atmospheres, 111 (D14), https://doi.org/10.1029/2005JD006655, 2006.

1250   Elguindi, N., Granier, C., Stavrakou, T., Darras, S., Bauwens, M., Cao, H., et al.: Intercomparison of magnitudes and trends in anthropogenic surface emissions from bottom-up inventories, top-down estimates and emission scenarios. Earth's Future, 8, e2020EF001520, https://doi.org/10.1029/2020EF001520, 2020.

1255   Emmons, L. K., Schwantes, R. H., Orlando, J. J., Tyndall, G., Kinnison, D., Lamarque, J.-F., et al.: The Chemistry Mechanism in the Community Earth System Model version 2 (CESM2). Journal of Advances in Modeling Earth Systems, 12, e2019MS001882. https://doi.org/10.1029/2019MS001882, 2020.

1260   Evensen, G.: The Ensemble Kalman Filter: Theoretical Formulation and Practical Implementation, Ocean Dynam., 53, 343–367, https://doi.org/10.1007/s10236-003-0036-9, 2003.

Feng, S., Jiang, F., Wu, Z., Wang, H., Ju, W., and Wang, H.: CO emissions inferred from surface CO observations over China in December 2013 and 2017. Journal of Geophysical Research: Atmospheres, 124. https://doi.org/10.1029/2019JD031808, 2020.

Foret, G., et al.: Ozone pollution: What can we see from space? A case study, J. Geophys. Res. Atmos.,119,8476–8499, https://doi.org/10.1002/2013JD021340, 2014.

Fortems-Cheiney, A., Chevallier, F., Pison, I., Bousquet, P., Szopa, S., Deeter, M. N., and Clerbaux, C.: Ten years of CO emissions as seen from Measurements of Pollution in the Troposphere (MOPITT), J. Geophys. Res., 116, D05304, https://doi.org/10.1029/2010JD014416, 2011.

Fortems-Cheiney, A., Chevallier, F., Pison, I., Bousquet, P., Saunois, M., Szopa, S., Cressot, C., Kurosu, T. P., Chance, K., and Fried, A.: The formaldehyde budget as seen by a global-scale multiconstraint and multi-species inversion system, Atmos. Chem. Phys., 12, 6699–6721, https://doi.org/10.5194/acp-12-6699-2012, 2012.

Fox, A.M., Hoar, T.J., Anderson, J.L., Arellano, A.F., Smith, W.K., Litvak, M.E., MacBean, N., Schimel, D.S., Moore, D.J.P.: Evaluation of a Data Assimilation System for Land Surface Models using CLM4.5. Journal of Advances in Modeling Earth Systems, 10, 2471–2494. https://doi.org/10.1002/2018MS001362, 2018.

Fu, D., Bowman, K. W., Worden, H., Natraj, V., Yu, S., Worden, J. R., et al.: High resolution tropospheric carbon monoxide profiles retrieved from CrIS and TROPOMI. Atmospheric Measurement Techniques, 9, 2567–2579, https://doi.org/10.5194/amt-9-2567-2016, 2016.

Ganzeveld, L., Valverde-Canossa, J., Moortgat, G. K., and Steinbrecher, R.: Evaluation of peroxide exchanges over a coniferous forest in a single-column chemistry-climate model, Atmos. Environ. 40, S68–S80, https://doi.org/10.1016/j.atmosenv.2006.01.062, 2006.

Gaubert, B., Coman, A., Foret, G., Meleux, F., Ung, A., Rouil, L., Ionescu, A., Candau, Y., and Beekmann, M.: Regional scale ozone data assimilation using an ensemble Kalman filter and the CHIMERE chemical transport model, Geosci. Model Dev., 7, 283-302, https://doi.org/10.5194/gmd-7-283-2014, 2014.

Gaubert, B., Arellano, A.F., Barré, J., Worden, H.M., Emmons, L.K., Tilmes, S., Buchholz, R.R., Vitt, F., Raeder, K., Collins, N., Anderson, J.L., Wiedinmyer, C., Martínez-Alonso, S., Edwards, D. P., Andreae, M. O., Hannigan, J. W., Petri, C., Strong, K., and Jones, N.: Toward a chemical reanalysis in a coupled chemistry-climate model: An evaluation of MOPITT CO assimilation and its impact on tropospheric composition. Journal of Geophysical Research: Atmospheres, 121(12), pp.7310-7343, https://doi.org/10.1002/2016JD024863, 2016.

Gaubert, B., H. M. Worden, A. F. J. Arellano, L. K. Emmons, S. Tilmes, J. Barré, S. Martinez Alonso, F. Vitt, J. L. Anderson, F. Alkemade, S. Houweling, Edwards D. P.: Chemical feedback from decreasing carbon monoxide emissions. Geophysical Research Letters, 44, 9985–9995, https://doi.org/10.1002/2017GL074987, 2017.

Gaubert, B., Stephens, B. B., Basu, S., Chevallier, F., Deng, F., Kort, E. A., Patra, P. K., Peters, W., Rödenbeck, C., Saeki, T., Schimel, D., Van der Laan-Luijkx, I., Wofsy, S., and Yin, Y.: Global

atmospheric CO2 inverse models converging on neutral tropical land exchange, but disagreeing on fossil fuel and atmospheric growth rate, Biogeosciences, 16, 117-134, https://doi.org/10.5194/bg-16-117-2019, 2019.

1315

Gettelman, A., Mills, M. J., Kinnison, D. E., Garcia, R. R., Smith, A. K., Marsh, D. R., et al.: The Whole Atmosphere Community Climate Model Version 6 (WACCM6). J. Geophys. Res. Atmos., 124. https://doi.org/10.1029/2019JD030943, 2019.

El Gharamti, M.: Enhanced adaptive inflation algorithm for ensemble filters. Mon. Wea. Rev.,
1320   146, 623–640, https://doi.org/10.1175/MWR-D-17-0187.1, 2018.

Guenther, A. B., X. Jiang, C. L. Heald, T. Sakulyanontvittaya, T. Duhl, L. K. Emmons, and Wang X.: The Model of Emissions of Gases and Aerosols from Nature version 2.1 (MEGAN2.1): An extended and updated framework for modeling biogenic emissions, Geosci. Model Dev., 5, 1471–
1325   1492, https://doi.org/10.5194/gmd-5-1471-2012, 2012.

Granier, C., S. Darras, H. Denier van der Gon, J. Doubalova, N. Elguindi, B. Galle, M. Gauss, M. Guevara, J.-P. Jalkanen, J. Kuenen, C. Liousse, B. Quack, D. Simpson, and Sindelarova K.: The Copernicus Atmosphere Monitoring Service global and regional emissions (April 2019 version).
1330   Copernicus Atmosphere Monitoring Service. https://doi.org/10.24380/D0BN-KX16, 2019.

Ha, S., Liu, Z., Sun, W., Lee, Y., and Chang, L.: Improving air quality forecasting with the assimilation of GOCI aerosol optical depth (AOD) retrievals during the KORUS-AQ period, Atmos. Chem. Phys., 20, 6015–6036, https://doi.org/10.5194/acp-20-6015-2020, 2020.

1335

Hall, B. and Claiborn, C.: Measurements of the dry deposition of peroxides to a Canadian boreal forest, J. Geophys. Res, 102, 29343–29353, https://doi.org/10.1029/97JD01113, 1997.

Hall, B., Claiborn, C., and Baldocchi, D.: Measurement and modeling of the dry deposition of
1340   peroxides, Atmos. Environ., 33, 577–589, https://doi.org/10.1016/S1352-2310(98)00271-4, 1999.

Halliday, H.S., Digangi, J.P., Choi, Y., et al.: Using short-term CO/CO_2 ratios to assess air mass differences over the Korean Peninsula during KORUS-AQ. J. Geophys. Res. https://doi.org/10.1029/2018JD029697, 2019.

1345

Heald, C. L., D. J. Jacob, D. B. A. Jones, P. I. Palmer, J. A. Logan, D. G. Streets, G.W. Sachse, J. C. Gille, R. N. Hoffman, and Nehrkorn T.: Comparative inverse analysis of satellite (MOPITT) and aircraft (TRACE-P) observations to estimate Asian sources of carbon monoxide, J. Geophys. Res., 109, D15S04, https://doi.org/10.1029/2004JD005185, 2004.

1350

Heald, C. L., Jacob, D. J., Park, R. J., Alexander, B., Fairlie, T. D., Yantosca, R. M., & Chu, D. A.: Transpacific transport of Asian anthropogenic aerosols and its impact on surface air quality in the United States. Journal of Geophysical Research, 111, D14310. https://doi.org/10.1029/2005JD006847, 2006.

1355

Herman, J., Spinei, E., Fried, A., Kim, J., Kim, J., Kim, W., Cede, A., Abuhassan, N., and Segal-Rozenhaimer, M.: NO2 and HCHO measurements in Korea from 2012 to 2016 from Pandora spectrometer instruments compared with OMI retrievals and with aircraft measurements during the KORUS-AQ campaign. Atmos. Meas. Tech., 11, 4583-4603, https://doi.org/10.5194/amt-11-
1360   4583-2018, 2018.

Hedelius, J. K., He, T.-L., Jones, D. B. A., Baier, B. C., Buchholz, R. R., De Mazière, M., Deutscher, N. M., Dubey, M. K., Feist, D. G., Griffith, D. W. T., Hase, F., Iraci, L. T., Jeseck, P., Kiel, M., Kivi, R., Liu, C., Morino, I., Notholt, J., Oh, Y.-S., Ohyama, H., Pollard, D. F., Rettinger, M., Roche, S., Roehl, C. M., Schneider, M., Shiomi, K., Strong, K., Sussmann, R., Sweeney, C., Té, Y., Uchino, O., Velazco, V. A., Wang, W., Warneke, T., Wennberg, P. O., Worden, H. M., and Wunch, D.: Evaluation of MOPITT Version 7 joint TIR–NIR X_{CO} retrievals with TCCON, Atmos. Meas. Tech., 12, 5547–5572, https://doi.org/10.5194/amt-12-5547-2019, 2019.

Hodzic, A., Kasibhatla, P. S., Jo, D. S., Cappa, C. D., Jimenez, J. L., Madronich, S., and Park, R. J.: Rethinking the global secondary organic aerosol (SOA) budget: stronger production, faster removal, shorter lifetime. Atmos. Chem. Phys., 16, 7917–7941, https://doi.org/10.5194/acp-16-7917-2016, 2016.

Hoesly, R. M., Smith, S. J., Feng, L., Klimont, Z., Janssens-Maenhout, G., Pitkanen, T., Seibert, J. J., Vu, L., Andres, R. J., Bolt, R. M., Bond, T. C., Dawidowski, L., Kholod, N., Kurokawa, J.-I., Li, M., Liu, L., Lu, Z., Moura, M. C. P., O'Rourke, P. R., and Zhang, Q.: Historical (1750–2014) anthropogenic emissions of reactive gases and aerosols from the Community Emissions Data System (CEDS), Geosci. Model Dev., 11, 369–408, https://doi.org/10.5194/gmd-11-369-2018, 2018.

Huang, M., Crawford, J. H., Diskin, G. S., Santanello, J. A., Kumar, S. V., Pusede, S. E., et al.: Modeling regional pollution transport events during KORUS-AQ: Progress and challenges in improving representation of land-atmosphere feedbacks. Journal of Geophysical Research: Atmospheres, 123, 10,732–10,756. https://doi.org/10.1029/2018JD028554, 2018.

Hunt, B. R., Kostelich, E. J., and Szunyogh, I.: Efficient data assimilation for spatiotemporal chaos: a local ensemble transform Kalman filter, Physica D, 230, 112–126, https://doi.org/10.1016/j.physd.2006.11.008, 2007.

Jacob, D. J., Logan, J. A., & Murti, P. P.: Effect of rising Asian emissions on surface ozone in the United States. Geophysical Research Letters, 26(14), 2175–2178, https://doi.org/10.1029/1999gl900450, 1999.

Jacob, D. J.: Heterogeneous chemistry and tropospheric ozone, Atmos. Environ., 34, 2131–2159, https://doi.org/10.1016/S1352-2310(99)00462-8, 2000.

Jaeglé, L., Jacob, D. J., Brune, W. H., Faloona, I., Tan, D., Heikes, B. G., Kondo, Y., Sachse, G. W., Anderson, B., Gregory, G. L., Singh, H. B., Pueschel, R., Ferry, G., Blake, D. R., and Shetter, R. E.: Photochemistry of HOx in the upper troposphere at northern midlatitudes, J. Geophys. Res., 105, 3877–3892, https://doi.org/10.1029/1999JD901016, 2000.

Jang, Y, Lee, Y, Kim, J, Kim, Y and Woo, J-H.: Improvement China Point Source for Improving Bottom-Up Emission Inventory. *Asia-Pacific Journal of Atmospheric Sciences*. DOI: 10.1007/s13143-019-00115-y, 2019.

Janssens-Maenhout, G., Crippa, M., Guizzardi, D., Dentener, F., Muntean, M., Pouliot, G., Keating, T., Zhang, Q., Kurokawa, J., Wankmüller, R., Denier van der Gon, H., Kuenen, J. J. P., Klimont, Z., Frost, G., Darras, S., Koffi, B., and Li, M.: HTAP_v2.2: a mosaic of regional and

1410   global emission grid maps for 2008 and 2010 to study hemispheric trans port of air pollution, Atmos. Chem. Phys., 15, 11411–11432, https://doi.org/10.5194/acp-15-11411-2015, 2015.

Jiang, Z., D. Jones, B. A., Kopacz, M., Liu, J., Henze, D. K., and Heald, C.: Quantifying the impact of model errors on top-down estimates of carbon monoxide emissions using satellite observations,
1415   J. Geophys. Res., 116, D15306, https://doi.org/10.1029/2010JD015282, 2011.

Jiang, Z., Jones, D. B. A., Worden, H. M., Deeter, M. N., Henze, D. K., Worden, J., Bowman, K. W., Brenninkmeijer, C. A. M., and Schuck, T. J.: Impact of model errors in convective transport on CO source estimates inferred from MOPITT CO retrievals, J. Geophys. Res. Atmos., 118,
1420   2073–2083, https://doi.org/10.1002/jgrd.50216, 2013.

Jiang, Z., Jones, D. B. A., Worden, H. M., and Henze, D. K.: Sensitivity of top-down CO source estimates to the modeled vertical structure in atmospheric CO, Atmos. Chem. Phys., 15, 1521–1537, https://doi.org/10.5194/acp-15-1521-2015, 2015.
1425

Kanaya, Y., Pochanart, P., Liu, Y., Li, J., Tanimoto, H., Kato, S., Suthawaree, J., Inomata, S., Taketani, F., Okuzawa, K., Kawamura, K., Akimoto, H., and Wang, Z. F.: Rates and regimes of photochemical ozone production over Central East China in June 2006: a box model analysis using comprehensive measurements of ozone precursors, Atmos. Chem. Phys., 9, 7711–7723,
1430   https://doi.org/10.5194/acp-9-7711-2009, 2009.

Kang, J.-S., E. Kalnay, J. Liu, I. Fung, T. Miyoshi, and Ide K.: "Variable localization" in an ensemble Kalman filter: Application to the carbon cycle data assimilation, J. Geophys. Res., 116, D09110, https://doi.org/10.1029/2010JD014673, 2011.
1435

Karspeck, A. R., Danabasoglu, G., Anderson, J., Karol, S., Collins, N., Vertenstein, M., Raeder, K., Hoar, T., Neale, R., Edwards, J., & Craig, A.: A global coupled ensemble data assimilation system using the Community Earth System Model and the Data Assimilation Research Testbed. Quarterly Journal of the Royal Meteorological Society, 144(717), 2404–2430.
1440   https://doi.org/10.1002/qj.3308, 2018.

Khalil, M. A. K. and Rasmussen, R. A.: Global decrease in atmospheric carbon monoxide concentration, Nature, 370, 639–641, https://doi.org/10.1038/370639a0, 1994.

1445   Kim, H., Zhang, Q., and Heo, J.: Influence of intense secondary aerosol formation and long-range transport on aerosol chemistry and properties in the Seoul Metropolitan Area during spring time: results from KORUS-AQ, Atmos. Chem. Phys., 18, 7149-7168, https://doi.org/10.5194/acp-18-7149-2018, 2018.

1450   Kim, H. C., Kim, S., Kim, B.-U., Jin, C.-S., Hong, S., Park, R., Son, S.-W., Bae, C., Bae, M., Song, C.-K. and Stein, A.: Recent increase of surface particulate matter concentrations in the Seoul Metropolitan Area, Korea. Scientific Report, 7, 4710, https://doi.org/10.1038/s41598-017-05092-8, 2017.

1455   Kim, H.-K., Woo, J.-H., Park, R. S., Song, C. H., Kim, J.-H., Ban, S.-J., and Park, J.-H.: Impacts of different plant functional types on ambient ozone predictions in the Seoul Metropolitan Areas (SMAs), Korea, Atmos. Chem. Phys., 14, 7461–7484, https://doi.org/10.5194/acp-14-7461-2014, 2014.

1460   Kim, H. K., Song C. K., Han K. M., Eo Y. D., Song C. H., Park R., Hong S.C., Kim S.K., Woo J.H.: Impact of biogenic emissions on early summer ozone and fine particulate matter exposure in the Seoul metropolitan area of Korea. Air Qual Atmos Health 11:1021–1035. https://doi.org/10.1007/s11869-018-0602-4, 2018.

1465   Kim, S., Kim, S.-Y., Lee, M., Shim, H., Wolfe, G. M., Guenther, A. B., He, A., Hong, Y., and Han, J.: Impact of isoprene and HONO chemistry on ozone and OVOC formation in a semirural South Korean forest, Atmos. Chem. Phys., 15, 4357–4371, https://doi.org/10.5194/acp-15-4357-2015, 2015.

1470   Kim, S., Sanchez, D., Wang, M., Seco, R., Jeong, D., Hughes, S., Barletta, B., Blake, D. R., Jung, J., Kim, D., Lee, G., Lee, M., Ahn, J., Lee, S. D., Cho, G., Sung, M. Y., Lee, Y. H., Kim, D. B., Kim, Y., Woo, J. H., Jo, D., Park, R., Park, J. H., Hong, Y. D., and Hong, J. H.: OH reactivity in urban and suburban regions in Seoul, South Korea-an East Asian megacity in a rapid transition, Faraday Dicuss., 189, 231–251, https://doi.org/10.1039/c5fd00230c, 2016.

1475

Kim, S. Y., Jiang, X., Lee, M., Turnipseed, A., Guenther, A., Kim, J.C., Lee, S.J. and Kim, S.: Impact of Biogenic Volatile Organic Compounds on ozone production at the Taehwa Research Forest near Seoul, South Korea. Atmos. Environ. 70: 447–453, https://doi.org/10.1016/j.atmosenv.2012.11.005, 2013.

1480

Kong, L., Tang, X., Zhu, J., Wang, Z., Fu, J. S., Wang, X., Itahashi, S., Yamaji, K., Nagashima, T., Lee, H.-J., Kim, C.-H., Lin, C.-Y., Chen, L., Zhang, M., Tao, Z., Li, J., Kajino, M., Liao, H., Wang, Z., Sudo, K., Wang, Y., Pan, Y., Tang, G., Li, M., Wu, Q., Ge, B., and Carmichael, G. R.: Evaluation and uncertainty investigation of the NO2, CO and NH3 modeling over China under the
1485   framework of MICS-Asia III, Atmos. Chem. Phys., 20, 181–202, https://doi.org/10.5194/acp-20-181-2020, 2020.

Kopacz, M., Jacob, D. J., Henze, D. K., Heald, C. L., Streets, D. G., and Zhang, Q.: Comparison of adjoint and analytical Bayesian inversion methods for constraining Asian sources of carbon
1490   monoxide using satellite (MOPITT) measurements of CO columns, J. Geophys. Res., 114, D04305, https://doi.org/10.1029/2007JD009264, 2009.

Kopacz, M., Jacob, D. J., Fisher, J. A., Logan, J. A., Zhang, L., Megretskaia, I. A., Yantosca, R. M., Singh, K., Henze, D. K., Burrows, J. P., Buchwitz, M., Khlystova, I., McMillan, W. W., Gille,
1495   J. C., Edwards, D. P., Eldering, A., Thouret, V., and Nedelec, P.: Global estimates of CO sources with high resolution by adjoint inversion of multiple satellite datasets (MOPITT, AIRS, SCIAMACHY, TES), Atmos. Chem. Phys., 10, 855–876, https://doi.org/10.5194/acp-10-855-2010, 2010.

1500   Kuze, A., Suto, H., Nakajima, M., and Hamazaki, T.: Thermal and near infrared sensor for carbon observation Fourier- transform spectrometer on the Greenhouse Gases Observing Satellite for greenhouse gases monitoring, Appl. Opt., 48, 6716, https://doi.org/10.1364/ao.48.006716, 2009.

Lamb, K. D., Perring, A. E., Samset, B., Peterson, D., Davis, S., Anderson, B. E., et al.: Estimating
1505   source region influences on black carbon abundance, microphysics, and radiative effect observed over South Korea. Journal of Geophysical Research: Atmospheres,123,13,527–13,548. https://doi.org/10.1029/2018JD029257, 2018.

Lee, H.-J., Jo, H.-Y., Park, S.-Y., Jo, Y.-J., Jeon, W., Ahn, J.-Y., and Kim, C.-H.: A case study of the transport/transformation of air pollutants over the Yellow Sea during the MAPS 2015 campaign. Journal of Geophysical Research: Atmospheres, 124, 6532–6553, https://doi.org/10.1029/2018JD029751, 2019a.

Lee, H.-J., Jo, H.-Y., Kim, S. et al.: Impacts of atmospheric vertical structures on transboundary aerosol transport from China to South Korea. Sci Rep 9, 13040, https://doi.org/10.1038/s41598-019-49691-z, 2019b.

Lee, K., Yu, J., Lee, S., Park, M., Hong, H., Park, S. Y., Choi, M., Kim, J., Kim, Y., Woo, J.-H., Kim, S.-W., and Song, C. H.: Development of Korean Air Quality Prediction System version 1 (KAQPS v1) with focuses on practical issues, Geosci. Model Dev., 13, 1055–1073, https://doi.org/10.5194/gmd-13-1055-2020, 2020.

Lelieveld, J., Gromov, S., Pozzer, A., and Taraborrelli, D.: Global tropospheric hydroxyl distribution, budget and reactivity, Atmos. Chem. Phys., 16, 12477–12493, https://doi.org/10.5194/acp-16-12477-2016, 2016.

Li, K., Jacob, D. J., Liao, H., Shen, L., Zhang, Q., and Bates K. H.: Anthropogenic drivers of 2013–2017 trends in summer 750 surface ozone in China, Proc. Natl. Acad. Sci. U. S. A., 116, 422-427, http://doi/.org/10.1073/pnas.1812168116, 2019.

Li, M., Zhang, Q., Kurokawa, J.-I., Woo, J.-H., He, K., Lu, Z., Ohara, T., Song, Y., Streets, D. G., Carmichael, G. R., Cheng, Y., Hong, C., Huo, H., Jiang, X., Kang, S., Liu, F., Su, H., and Zheng, B.: MIX: a mosaic Asian anthropogenic emission inventory under the international collaboration framework of the MICS-Asia and HTAP, Atmos. Chem. Phys., 17, 935–963, https://doi.org/10.5194/acp-17-935-2017, 2017.

Li, M., Q. Zhang, B. Zheng, D. Tong, Y. Lei, et al.: Persistent growth of anthropogenic non-methane volatile organic compound (NMVOC) emissions in China during 1990–2017: drivers, speciation and ozone formation potential. Atmospheric Chemistry and Physics, 19:8897–8913, https://doi.org/10.5194/acp-19-8897-2019, 2019.

Li, Z. Q., et al.: Aerosol and boundary-layer interactions and impact on air quality, National Science Review, 4(6), 810-833, https://doi.org/10.1093/nsr/nwx117, 2017.

Liu, L., Zhuang, Q., Zhu, Q., Liu, S., van Asperen, H., and Pihlatie, M.: Global soil consumption of atmospheric carbon monoxide: an analysis using a process-based biogeochemistry model, Atmos. Chem. Phys., 18, 7913–7931, https://doi.org/10.5194/acp-18-7913-2018, 2018.

Lim, Y. J., Armendariz, A., Son, Y. S., and Kim, J. C.: Seasonal variations of isoprene emissions from five oak tree species in East Asia, Atmos. Environ., 45, 2202–2210, https://doi.org/10.1016/J.Atmosenv.2011.01.066, 2011.

Lin, M., et al.: Transport of Asian ozone pollution into surface air over the western United States in spring, J. Geophys. Res.,117, D00V07, https://doi.org/10.1029/2011JD016961, 2012.

Maksyutov, S., Oda, T., Saito, M., Janardanan, R., Belikov, D., Kaiser, J. W., Zhuravlev, R., Ganshin, A., Valsala, V. K., Andrews, A., Chmura, L., Dlugokencky, E., Haszpra, L., Langenfelds, R. L., Machida, T., Nakazawa, T., Ramonet, M., Sweeney, C., and Worthy, D.: Technical note: A high-resolution inverse modelling technique for estimating surface CO_2 fluxes based on the NIES-TM – FLEXPART coupled transport model and its adjoint, Atmos. Chem. Phys. Discuss., https://doi.org/10.5194/acp-2020-251, in review, 2020.

Matthes, K., Funke, B., Andersson, M. E., Barnard, L., Beer, J., Charbonneau, P., Clilverd, M. A., Dudok de Wit, T., Haberreiter, M., Hendry, A., Jackman, C. H., Kretzschmar, M., Kruschke, T., Kunze, M., Langematz, U., Marsh, D. R., Maycock, A. C., Misios, S., Rodger, C. J., Scaife, A. A., Seppälä, A., Shangguan, M., Sinnhuber, M., Tourpali, K., Usoskin, I., van de Kamp, M., Verronen, P. T., and Versick, S.: Solar forcing for CMIP6 (v3.2), Geosci. Model Dev., 10, 2247–2302, https://doi.org/10.5194/gmd-10-2247-2017, 2017.

Meinshausen, M., Vogel, E., Nauels, A., Lorbacher, K., Meinshausen, N., Etheridge, D. M., Fraser, P. J., Montzka, S. A., Rayner, P. J., Trudinger, C. M., Krummel, P. B., Beyerle, U., Canadell, J. G., Daniel, J. S., Enting, I. G., Law, R. M., Lunder, C. R., O'Doherty, S., Prinn, R. G., Reimann, S., Rubino, M., Velders, G. J. M., Vollmer, M. K., Wang, R. H. J., and Weiss, R.: Historical greenhouse gas concentrations for climate modelling (CMIP6), Geosci. Model Dev., 10, 2057–2116, https://doi.org/10.5194/gmd-10-2057-2017, 2017.

Mills, M. J., Schmidt, A., Easter, R., Solomon, S., Kinnison, D. E., Ghan, S. J., et al.: Global volcanic aerosol properties derived from emissions, 1990–2014, using CESM1(WACCM). Journal of Geophysical Research: Atmospheres, 121, 2332–2348. https://doi.org/10.1002/2015JD024290, 2016.

Miyazaki, K., Eskes, H. J., Sudo, K., Takigawa, M., van Weele, M., and Boersma, K. F.: Simultaneous assimilation of satellite NO2, O3, CO, and HNO3 data for the analysis of tropospheric chemical composition and emissions, Atmos. Chem. Phys., 12, 9545–9579, https://doi.org/10.5194/acp-12-9545-2012, 2012.

Miyazaki, K., Eskes, H. J., and Sudo, K.: A tropospheric chemistry reanalysis for the years 2005–2012 based on an assimilation of OMI, MLS, TES, and MOPITT satellite data, Atmos. Chem. Phys., 15, 8315–8348, https://doi.org/10.5194/acp-15-8315-2015, 2015.

Miyazaki, K., Eskes, H., Sudo, K., Boersma, K. F., Bowman, K., and Kanaya, Y.: Decadal changes in global surface NOx emissions from multi-constituent satellite data assimilation, Atmos. Chem. Phys., 17, 807–837, https://doi.org/10.5194/acp-17-807-2017, 2017.

Miyazaki, K., Sekiya, T., Fu, D., Bowman, K. W., Kulawik, S. S., Sudo, K., Walker, T., Kanaya, Y., Takigawa, M., Ogochi, K., Eskes, H., Boersma, K. F., Thompson, A. M., Gaubert, B., Barre, J., and Emmons, L. K.: Balance of emission and dynamical controls on ozone during KORUS-AQ from multi-constituent satellite data assimilation, J. Geophys. Res.-Atmos., 124, 387–413, https://doi.org/10.1029/2018JD028912, 2019a.

Miyazaki, K., Bowman, K., Sekiya, T., Eskes, H., Boersma, F., Worden, H., Livesey, N., Payne, V. H., Sudo, K., Kanaya, Y., Takigawa, M., and Ogochi, K.: Chemical Reanalysis Products. Jet Propulsion Laboratory. https://doi.org/10.25966/9qgv-fe81, 2019b.

Miyazaki, K., Bowman, K. W., Yumimoto, K., Walker, T., and Sudo, K.: Evaluation of a multi-model, multi-constituent assimilation framework for tropospheric chemical reanalysis, Atmos. Chem. Phys., 20, 931–967, https://doi.org/10.5194/acp-20-931-2020, 2020a.

Miyazaki, K., Bowman, K., Sekiya, T., Eskes, H., Boersma, F., Worden, H., Livesey, N., Payne, V. H., Sudo, K., Kanaya, Y., Takigawa, M., and Ogochi, K.: Updated tropospheric chemistry reanalysis and emission estimates, TCR-2, for 2005–2018, Earth Syst. Sci. Data, 12, 2223–2259, https://doi.org/10.5194/essd-12-2223-2020, 2020b.

Molod, A., Takacs, L., Suarez, M., & Bacmeister, J.: Development of the GEOS-5 atmospheric general circulation model: evolution from MERRA to MERRA2. Geoscientific Model Development, 8(5), 1339-1356. https://doi.org/10.5194/gmd-8-1339-2015, 2015.

Montzka, S. A., Krol, M., Dlugokencky, E., Hall, B., Jöckel, P., and Lelieveld, J.: Small Interannual Variability of Global Atmospheric Hydroxyl, Science, 331, 67–69, https://doi.org/10.1126/science.1197640, 2011.

Müller, M., Mikoviny, T., Feil, S., Haidacher, S., Hanel, G., Hartungen, E., Jordan, A., Märk, L., Mutschlechner, P., Schottkowsky, R., Sulzer, P., Crawford, J. H., and Wisthaler, A.: A compact PTR-ToF-MS instrument for airborne measurements of volatile organic compounds at high spatiotemporal resolution, Atmos. Meas. Tech., 7, 3763–3772, https://doi.org/10.5194/amt-7-3763-2014, 2014.

Müller, J.-F., Stavrakou, T., Bauwens, M., George, M., Hurtmans, D., Coheur, P.-F., Clerbaux, C., and Sweeney, C.: Top-Down CO Emissions Based On IASI Observations and Hemispheric Constraints on OH Levels, Geophys. Res. Lett., 45, 1621–1629, https://doi.org/10.1002/2017GL076697, 2018.

Myhre, G.; Shindell, D.; et al.: Anthropogenic and Natural Radiative Forcing. The Physical Science Basis. Contribution of Working Group I to the Fifth Assessment Report of the Intergovernmental Panel on Climate Change 2013, Cambridge, United Kingdom and New York, NY, USA: Cambridge University Press http://www.ipcc.ch/pdf/assessment-report/ar5/wg1/WG1AR5_Chapter08_FINAL.pdf, 2013.

Naik, V., Voulgarakis, A., Fiore, A. M., Horowitz, L. W., Lamarque, J.-F., Lin, M., Prather, M. J., Young, P. J., Bergmann, D., Cameron-Smith, P. J., Cionni, I., Collins, W. J., Dalsøren, S. B., Doherty, R., Eyring, V., Faluvegi, G., Folberth, G. A., Josse, B., Lee, Y. H., MacKenzie, I. A., Nagashima, T., van Noije, T. P. C., Plummer, D. A., Righi, M., Rumbold, S. T., Skeie, R., Shindell, D. T., Stevenson, D. S., Strode, S., Sudo, K., Szopa, S., and Zeng, G.: Preindustrial to present-day changes in tropospheric hydroxyl radical and methane lifetime from the Atmospheric Chemistry and Climate Model Intercomparison Project (ACCMIP), Atmos. Chem. Phys., 13, 5277–5298, https://doi.org/10.5194/acp-13-5277-2013, 2013.

National Academies of Sciences, Engineering, and Medicine: The Future of Atmospheric Chemistry Research: Remembering Yesterday, Understanding Today, Anticipating Tomorrow, The National Academies Press, Washington DC, USA, https://doi.org/10.17226/23573, 2016.

Nault, B. A., Campuzano-Jost, P., Day, D. A., Schroder, J. C., Anderson, B., Beyersdorf, A. J., Blake, D. R., Brune, W. H., Choi, Y., Corr, C. A., de Gouw, J. A., Dibb, J., DiGangi, J. P., Diskin,

G. S., Fried, A., Huey, L. G., Kim, M. J., Knote, C. J., Lamb, K. D., Lee, T., Park, T., Pusede, S. E., Scheuer, E., Thornhill, K. L., Woo, J.-H., and Jimenez, J. L.: Secondary organic aerosol production from local emissions dominates the organic aerosol budget over Seoul, South Korea, during KORUS-AQ, Atmos. Chem. Phys., 18, 17769-17800, https://doi.org/10.5194/acp-18-17769-2018, 2018.

Nguyen, N. H., Turner, A. J., Yin, Y., Prather, M. J., & Frankenberg, C.: Effects of Chemical Feedbacks on Decadal Methane Emissions Estimates. Geophysical Research Letters, 47, e2019GL085706, https://doi.org/10.1029/2019GL085706, 2020.

Nguyen, T. B., Crounse, J. D., Teng, A. P., St Clair, J. M., Paulot, F., Wolfe, G. M., and Wennberg, P. O.: Rapid deposition of oxidized biogenic compounds to a temperate forest, P. Natl. Acad. Sci USA, 112, 392–401, https://doi.org/10.1073/pnas.1418702112, 2015.

Oak, Y.J., Park, R.J., Schroeder, J.R., Crawford, J.H., Blake, D.R., Weinheimer, A.J., Woo, J.-H., Kim, S.-W., Yeo, H., Fried, A., Wisthaler, A. and Brune, W.H.: Evaluation of simulated O3 production efficiency during the KORUS-AQ campaign: Implications for anthropogenic NOx emissions in Korea. Elem Sci Anth, 7(1), p.56. DOI: http://doi.org/10.1525/elementa.394, 2019.

Patra, P. K., Houweling, S., Krol, M., Bousquet, P., Belikov, D., Bergmann, D., Bian, H., Cameron-Smith, P., Chipperfield, M. P., Corbin, K., Fortems-Cheiney, A., Fraser, A., Gloor, E., Hess, P., Ito, A., Kawa, S. R., Law, R. M., Loh, Z., Maksyutov, S., Meng, L., Palmer, P. I., Prinn, R. G., Rigby, M., Saito, R., and Wilson, C.: TransCom model simulations of CH4 and related species: linking transport, surface flux and chemical loss with CH4 variability in the troposphere and lower stratosphere, Atmos. Chem. Phys., 11, 12813–12837, https://doi.org/10.5194/acp-11-12813-2011, 2011.

Pandey, S., Houweling, S., Krol, M., Aben, I., Chevallier, F., Dlugokencky, E. J., Gatti, L. V., Gloor, M., Miller, J. B., Detmers, R., Machida, T., and Röckmann, T.: Inverse modeling of GOSAT-retrieved ratios of total column CH4 and CO2 for 2009 and 2010, Atmos. Chem. Phys., 16, 5043–5062, https://doi.org/10.5194/acp-16-5043-2016, 2016.

Peterson, D.A., Hyer, E.J., Han, S.-O., Crawford, J.H., Park, R.J., Holz, R., Kuehn, R.E., Eloranta, E., Knote, C., Jordan, C.E. and Lefer, B.L.: Meteorology influencing springtime air quality, pollution transport, and visibility in Korea. Elem Sci Anth, 7(1), p.57. DOI: http://doi.org/10.1525/elementa.395, 2019.

Petropavlovskikh, I., Shetter, R., Hall, S., Ullmann, K., and Bhartia, P. K.: Algorithm for the charge-coupled-device scanning actinic flux spectroradiometer ozone retrieval in support of the Aura satellite validation, J. Appl. Remote Sens., 1, 013540, https://doi.org/10.1117/1.2802563, 2007.

Pétron, G., Granier, C., Khattatov, B., Yudin, V., Lamarque, J.-F., Emmons, L., Gille, J., and Edwards, D. P.: Monthly CO surface sources inventory based on the 2000–2001 MOPITT satellite data, Geophys. Res. Lett., 31, L21107, https://doi.org/10.1029/2004GL020560, 2004.

Pison, I., Bousquet, P., Chevallier, F., Szopa, S., and Hauglustaine, D.: Multi-species inversion of CH4, CO and H2 emissions from surface measurements, Atmos. Chem. Phys., 9, 5281–5297, https://doi.org/10.5194/acp-9-5281-2009, 2009.

Podolske, J. R., Sachse, G. W., and Diskin, G. S.: Calibration and data retrieval algorithms for the NASA Langley/Ames Diode Laser Hygrometer for the NASA Transport and Chemical Evolution Over the Pacific (TRACE-P) mission. Journal of Geophysical Research, 108(D20), 8792, https://doi.org/10.1029/2002JD003156, 2003.

Prather, M. J., & Holmes, C. D.: Overexplaining or underexplaining methane's role in climate change. Proceedings of the National Academy of Sciences, 114 (21), 5324–5326, https://doi.org/10.1073/pnas.1704884114, 2017.

Raeder, K., Anderson, J. L., Collins, N., Hoar, T. J., Kay, J. E., Lauritzen, P. H., and Pincus, R.: DART/CAM: an ensemble data assimilation system for CESM atmospheric models, J. Climate, 25, 6304–6317, https://doi.org/10.1175/JCLI-D-11-00395.1, 2012.

Richter, D., P. Weibring, J. G. Walega, A. Fried, S. M. Spuler, and M. S. Taubman, Compact highly sensitive multi-species airborne mid-IR spectrometer, Appl. Phys. B, 119 (1), 119-131, https://doi.org/10.1007/s00340-015-6038-8, 2015.

Ridley, B. A., and Grahek, F. E.: A small, low flow, high sensitivity reaction vessel for NO chemiluminescence detectors. Journal Of Atmospheric And Oceanic Technology, 7, 307-311, https://doi.org/10.1175/1520-0426(1990)007<0307:ASLFHS>2.0.CO;2, 1990.

Sachse, G. W., Hill, G. F., Wade, L. O., and Perry, M. G.: Fast response, high-precision carbon monoxide sensor using a tunable diode laser absorption technique, J. Geophys. Res., 92, 2071–2081, https://doi.org/10.1029/JD092iD02p02071,1987.

Saunois, M., Jackson, R. B., Bousquet, P., Poulter, B., and Canadell, J. G.: The growing role of methane in anthropogenic climate change. Environmental Research Letters, 11 (12), 120207. https://doi.org/10.1088/1748-9326/11/12/120207, 2016.

Saunois, M., Stavert, A. R., Poulter, B., Bousquet, P., Canadell, J. G., Jackson, R. B., Raymond, P. A., Dlugokencky, E. J., Houweling, S., Patra, P. K., Ciais, P., Arora, V. K., Bastviken, D., Bergamaschi, P., Blake, D. R., Brailsford, G., Bruhwiler, L., Carlson, K. M., Carrol, M., Castaldi, S., Chandra, N., Crevoisier, C., Crill, P. M., Covey, K., Curry, C. L., Etiope, G., Frankenberg, C., Gedney, N., Hegglin, M. I., Höglund-Isaksson, L., Hugelius, G., Ishizawa, M., Ito, A., Janssens-Maenhout, G., Jensen, K. M., Joos, F., Kleinen, T., Krummel, P. B., Langenfelds, R. L., Laruelle, G. G., Liu, L., Machida, T., Maksyutov, S., McDonald, K. C., McNorton, J., Miller, P. A., Melton, J. R., Morino, I., Müller, J., Murguia-Flores, F., Naik, V., Niwa, Y., Noce, S., O'Doherty, S., Parker, R. J., Peng, C., Peng, S., Peters, G. P., Prigent, C., Prinn, R., Ramonet, M., Regnier, P., Riley, W. J., Rosentreter, J. A., Segers, A., Simpson, I. J., Shi, H., Smith, S. J., Steele, L. P., Thornton, B. F., Tian, H., Tohjima, Y., Tubiello, F. N., Tsuruta, A., Viovy, N., Voulgarakis, A., Weber, T. S., van Weele, M., van der Werf, G. R., Weiss, R. F., Worthy, D., Wunch, D., Yin, Y., Yoshida, Y., Zhang, W., Zhang, Z., Zhao, Y., Zheng, B., Zhu, Q., Zhu, Q., and Zhuang, Q.: The Global Methane Budget 2000–2017, Earth Syst. Sci. Data, 12, 1561–1623, https://doi.org/10.5194/essd-12-1561-2020, 2020.

Segers, A.J.: Description of the CH4 Inversion Production Chain, CAMS (Copernicus Atmospheric Monitoring Service) Report, latest version:

https://atmosphere.copernicus.eu/sites/default/files/2020-01/CAMS73_2018SC1_D73.5.2.2-2019_202001_production_chain_v1.pdf, 2020

Shindell, D. T., Faluvegi, G., Stevenson, D. S., Krol, M. C., Emmons, L. K., Lamarque, J.-F., Petron, G., Dentener, F. J., Ellingsen, K., Schultz, M. G., Wild, O, Amann, M., Atherton, C. S., Bergmann, D. J., Bey, I., Butler, T., Cofala, J., Collins, W. J., Derwent, R. G., Doherty, R. M., Drevet, J., Eskes, H. J., Fiore, A. M., Gauss, M., Hauglustaine, D. A., Horowitz, L. W., Isaksen, S. A., Lawrence, M. G., Montanaro, V., Muller, J.-F., Pitari, G., Parther, M. J., Pyle, J. A., Rast, S., Rodriguez, J. M., Sanderson, M. G., Savage, N. H., Strahan, S. E., Sudo, K., Szopa, S., Unger, N., van Noije, T. P. C., and Zeng, G.: Multimodel simulations of carbon monoxide: Comparison with observations and projected near-future changes, J. Geophys. Res., 111, D19306, https://doi.org/10.1029/2006JD007100, 2006.

Shen, L., Jacob, D. J., Zhu, L., Zhang, Q., Zheng, B., Sulprizio, M. P., Li, K., De Smedt, I., González Abad, G., Cao, H., Fu, T.-M., and Liao, H.: 2005–2016 trends of formaldehyde columns over China observed by satellites: increasing anthropogenic emissions of volatile organic compounds and decreasing agricultural fire emissions, Geophys. Res. Lett., 46, 4468–4475, https://doi.org/10.1029/2019gl082172, 2019.

Shetter, R. E. and Müller, M.: Photolysis frequency measurements using actinic flux spectroradiometry during the PEM-Tropics mission: Instrumentation description and some results, J. Geophys. Res., 104, 5647–5661, https://doi.org/10.1029/98JD01381, 1999.

Simpson, I.J., Blake, D.R., Blake, N.J., Meinardi, S., Barletta, B., Hughes, S.C., Fleming, L.T., Crawford, J.H., Diskin, G.S., Emmons, L.K., Fried, A., Guo, H., Peterson, D.A., Wisthaler, A., Woo, J.-H., Barré, J., Gaubert, B., Kim, J., Kim, M.J., Kim, Y., Knote, C., Mikoviny, T., Pusede, S.E., Schroeder, J.R., Wang, Y., Wennberg, P.O. and Zeng, L.: Characterization, sources and reactivity of volatile organic compounds (VOCs) in Seoul and surrounding regions during KORUS-AQ, Elem. Sci. Anth., 8, 37, http://doi.org/10.1525/elementa.434, 2020.

Song, H., Chen, X., Lu, K., Zou, Q., Tan, Z., Fuchs, H., Wiedensohler, A., Zheng, M., Wahner, A., Kiendler-Scharr, A., and Zhang, Y.: Influence of aerosol copper on HO2 uptake: A novel parameterized equation, Atmos. Chem. Phys. Discuss., https://doi.org/10.5194/acp-2020-218, in review, 2020.

Souri, A. H., Nowlan, C. R., González Abad, G., Zhu, L., Blake, D. R., Fried, A., Weinheimer, A. J., Wisthaler, A., Woo, J.-H., Zhang, Q., Chan Miller, C. E., Liu, X., and Chance, K.: An inversion of NOx and non-methane volatile organic compound (NMVOC) emissions using satellite observations during the KORUS-AQ campaign and implications for surface ozone over East Asia, Atmos. Chem. Phys., 20, 9837–9854, https://doi.org/10.5194/acp-20-9837-2020, 2020.

Stavrakou, T., and Müller, J.-F.: Grid-based versus big region approach for inverting CO emissions using Measurement of Pollution in the Troposphere (MOPITT) data, J. Geophys. Res., 111, D15304, https://doi.org/10.1029/2005JD006896, 2006.

Stein, O., Schultz, M. G., Bouarar, I., Clark, H., Huijnen, V., Gaudel, A., George, M., and Clerbaux, C.: On the wintertime low bias of Northern Hemisphere carbon monoxide found in global model simulations, Atmos. Chem. Phys., 14, 9295–9316, https://doi.org/10.5194/acp-14-9295-2014, 2014.

1800

Strode, S. A., Duncan, B. N., Yegorova, E. A., Kouatchou, J., Ziemke, J. R., and Douglass, A. R.: Implications of carbon monoxide bias for methane lifetime and atmospheric composition in chemistry climate models, Atmos. Chem. Phys., 15, 11789–11805, https://doi.org/10.5194/acp-15-11789-2015, 2015.

1805

Sullivan, J. T., McGee, T. J., Stauffer, R. M., Thompson, A. M., Weinheimer, A., Knote, C., Janz, S., Wisthaler, A., Long, R., Szykman, J., Park, J., Lee, Y., Kim, S., Jeong, D., Sanchez, D., Twigg, L., Sumnicht, G., Knepp, T., & Schroeder, J. R.: Taehwa Research Forest: a receptor site for severe domestic pollution events in Korea during 2016, Atmos. Chem. Phys., 19, 5051-5067,
1810   https://doi.org/10.5194/acp-19-5051-2019, 2019.

Tang, W., Arellano, A. F., DiGangi, J. P., Choi, Y., Diskin, G. S., Agustí-Panareda, A., Parrington, M., Massart, S., Gaubert, B., Lee, Y., Kim, D., Jung, J., Hong, J., Hong, J.-W., Kanaya, Y., Lee, M., Stauffer, R. M., Thompson, A. M., Flynn, J. H., and Woo, J.-H.: Evaluating high-resolution
1815   forecasts of atmospheric CO and CO2 from a global prediction system during KORUS-AQ field campaign, Atmos. Chem. Phys., 18, 11007–11030, https://doi.org/10.5194/acp-18-11007-2018, 2018.

Tang, W., Emmons, L. K., Arellano Jr, A. F., Gaubert, B., Knote, C., Tilmes, S., et al.: Source
1820   contributions to carbon monoxide concentrations during KORUS-AQ based on CAM-chem model applications. Journal of Geophysical Research: Atmospheres, 124, 2796–2822. https://doi.org/10.1029/2018JD029151, 2019.

Tang, W., Worden, H. M., Deeter, M. N., Edwards, D. P., Emmons, L. K., Martínez-Alonso, S.,
1825   Gaubert, B., Buchholz, R. R., Diskin, G. S., Dickerson, R. R., Ren, X., He, H., and Kondo, Y.: Assessing Measurements of Pollution in the Troposphere (MOPITT) carbon monoxide retrievals over urban versus non-urban regions, Atmos. Meas. Tech., 13, 1337–1356, https://doi.org/10.5194/amt-13-1337-2020, 2020.

1830   Tang, X., Zhu, J., Wang, Z. F., Wang, M., Gbaguidi, A., Li, J., Shao, M., Tang, G. Q., and Ji, D. S.: Inversion of CO emissions over Beijing and its surrounding areas with ensemble Kalman filter, Atmos. Environ., 81, 676–686, https://doi.org/10.1016/j.atmosenv.2013.08.051, 2013.

Thompson, A. M., Stauffer, R. M., Boyle, T. P., Kollonige, D. E., Miyazaki, K., Tzortziou, M.,
1835   Herman, J. R., Jordan, C. N., Lamb, B. T., and Duncan, B. N.: Comparison of Near-Surface NO2 Pollution With Pandora Total Column NO2 During the Korea-United States Ocean Color (KORUS OC) Campaign, J. Geophys. Res.-Atmos., 124, 13560–13575, https://doi.org/10.1029/2019JD030765, 2019.

1840   Tilmes, S., Hodzic, A., Emmons, L. K., Mills, M. J., Gettelman, A., Kinnison, D. E., Park, M., Lamarque, J.-F., Vitt, F., Shrivastava, M., Campuzano-Jost, P., Jimenez, J. L., and Liu, X.: Climate forcing and trends of organic aerosols in the Community Earth System Model (CESM2), J. Adv. Model. Earth Syst., 11, 4323–4351, https://doi.org/10.1029/2019MS001827, 2019.

1845   Tsuruta, A., Aalto, T., Backman, L., Hakkarainen, J., van der Laan-Luijkx, I. T., Krol, M. C., Spahni, R., Houweling, S., Laine, M., Dlugokencky, E., Gomez-Pelaez, A. J., van der Schoot, M., Langenfelds, R., Ellul, R., Arduini, J., Apadula, F., Gerbig, C., Feist, D. G., Kivi, R., Yoshida, Y.,

and Peters, W.: Global methane emission estimates for 2000–2012 from CarbonTracker Europe-CH4 v1.0, Geosci. Model Dev., 10, 1261-1289, https://doi.org/10.5194/gmd-10-1261-2017, 2017.

Turner, A. J., Frankenberg, C. and & Kort, E. A.: Interpreting contemporary trends in atmospheric methane. Proceedings of the National Academy of Sciences, 116, 2805, https://doi.org/10.1073/pnas.1814297116, 2019.

Ganzeveld, L., Valverde-Canossa, J., Moortgat, G. K., and Steinbrecher, R.: Evaluation of peroxide exchanges over a coniferous forest in a single-column chemistry-climate model, Atmos. Environ. 40, S68–S80, https://doi.org/10.1016/j.atmosenv.2006.03.038, 2006.

Wang, F., Li, Z., Ren, X., Jiang, Q., He, H., Dickerson, R. R., Dong, X., and Lv, F.: Vertical distributions of aerosol optical properties during the spring 2016 ARIAs airborne campaign in the North China Plain, Atmos. Chem. Phys., 18, 8995–9010, https://doi.org/10.5194/acp-18-8995-2018, 2018.

Wang, F., Maksyutov, S., Tsuruta, A., Janardanan, R., Ito, A., Sasakawa, M., Machida, T., Morino, I., Yoshida, Y., Kaiser, J.W., et al.: Methane emission estimates by the global high-resolution inverse model using national inventories. Remote Sens. 11, 2489, https://doi.org/10.3390/rs11212489, 2019.

Wang T, et al.: Ozone pollution in China: A review of concentrations, meteorological influences, chemical precursors, and effects. Sci Total Environ 575:1582–1596, http://dx.doi.org/10.1016/j.scitotenv.2016.10.081, 2017.

Warner, J. X., Wei, Z., Strow, L. L., Barnet, C. D., Sparling, L. C., Diskin, G., and Sachse, G.: Improved agreement of AIRS tropospheric carbon monoxide products with other EOS sensors using optimal estimation retrievals, Atmos. Chem. Phys., 10, 9521–9533, https://doi.org/10.5194/acp-10-9521-2010, 2010.

Watanabe, S., Hajima, T., Sudo, K., Nagashima, T., Takemura, T., Okajima, H., Nozawa, T., Kawase, H., Abe, M., Yokohata, T., Ise, T., Sato, H., Kato, E., Takata, K., Emori, S., and Kawamiya, M.: MIROC-ESM 2010: model description and basic results of CMIP5-20c3m experiments, Geosci. Model Dev., 4, 845–872, https://doi.org/10.5194/gmd-4-845-2011, 2011.

Weinheimer, A. J., Walega, J. G., Ridley, B. A., Sachse, G. W., Anderson, B. E. and Collins, J. E.: Stratospheric NOy measurements on the NASA DC-8 during AASE-II. Geophysical Research Letters, 20, 2563–2566, https://doi.org/10.1029/93GL02627, 1993.

Wilkening, K. E., Barrie, L. A. & Engle, M.: Trans-pacific air pollution. Science, 290 (5489), 65–67, https://doi.org/10.1126/science.290.5489.65, 2000.

Woo, J-H, Choi, K-C, Kim, HK, Baek, BH, Jang, M, Eum, J-H, Song, CH, Ma, Y-l, Sunwoo, Y, Chang, L-S and Yood, SH.: Development of an anthropogenic emissions processing system for Asia using SMOKE. Atmospheric Environment 58: 5–13, https://doi.org/10.1016/j.atmosenv.2011.10.042, 2012.

1895   Worden, H. M., Deeter, M. N., Edwards, D. P., Gille, J. C., Drummond, J. R., and Nédélec, P.: Observations of near-surface carbon monoxide from space using MOPITT multispectral retrievals, J. Geophys. Res., 115, D18314, https://doi.org/10.1029/2010JD014242, 2010.

Worden, H. M., Deeter, M. N., Frankenberg, C., George, M., Nichitiu, F., Worden, J., Aben, I.,
1900   Bowman, K. W., Clerbaux, C., Coheur, P. F., de Laat, A. T. J., Detweiler, R., Drummond, J. R., Edwards, D. P., Gille, J. C., Hurtmans, D., Luo, M., Martínez-Alonso, S., Massie, S., Pfister, G., and Warner, J. X.: Decadal record of satellite carbon monoxide observations, Atmos. Chem. Phys., 13, 837–850, https://doi.org/10.5194/acp-13-837-2013, 2013.

1905   Yan, Y.-Y., Lin, J.-T., Kuang, Y., Yang, D., and Zhang, L.: Tropospheric carbon monoxide over the Pacific during HIPPO: two-way coupled simulation of GEOS-Chem and its multiple nested models, Atmos. Chem. Phys., 14, 12649–12663, https://doi.org/10.5194/acp-14-12649-2014, 2014.

1910   Yin, Y., Chevallier, F., Ciais, P., Broquet, G., Fortems-Cheiney, A., Pison, I., and Saunois, M.: Decadal trends in global CO emissions as seen by MOPITT, Atmos. Chem. Phys., 15, 13433–13451, https://doi.org/10.5194/acp-15-13433-2015, 2015.

Yin, Y., Chevallier, F., Frankenberg, C., Ciais, P., Bousquet, P., Saunois, M., Zheng, B., Worden,
1915   J. R., Bloom, A. A., Parker, R., Jacob, D., J., and Dlugokencky, E. J.: Sources from tropical wetlands and China accelerate methane growth rate since 2010, submitted to PNAS, 2019.

Yonemura, S., Kawashima, S., and Tsuruta, H.: Carbon monoxide, hydrogen, and methane uptake by soils in a temperate arable field and a forest, J. Geophys. Res., 105, 14347,
1920   https://doi.org/10.1029/1999JD901156, 2000.

Young, P. J., Archibald, A. T., Bowman, K. W., Lamarque, J.-F., Naik, V., Stevenson, D. S., Tilmes, S., Voulgarakis, A., Wild, O., Bergmann, D., Cameron-Smith, P., Cionni, I., Collins, W. J., Dalsøren, S. B., Doherty, R. M., Eyring, V., Faluvegi, G., Horowitz, L. W., Josse, B., Lee, Y.
1925   H., MacKenzie, I. A., Nagashima, T., Plummer, D. A., Righi, M., Rumbold, S. T., Skeie, R. B., Shindell, D. T., Strode, S. A., Sudo, K., Szopa, S., and Zeng, G.: Pre-industrial to end 21st century projections of tropospheric ozone from the Atmospheric Chemistry and Climate Model Intercomparison Project (ACCMIP), Atmos. Chem. Phys., 13, 2063–2090, https://doi.org/10.5194/acp-13-2063-2013, 2013.
1930

Yumimoto, K., Uno, I., and Itahashi, S.: Long-term inverse modeling of Chinese CO emission from satellite observations, Environmental Pollution, 195, 308–318, https://doi.org/10.1016/j.envpol.2014.07.026, 2014.

1935   Zhang, L., et al.: Transpacific transport of ozone pollution and the effect of recent Asian emission increases on air quality in North America: An integrated analysis using satellite, aircraft, ozonesonde, and surface observations, Atmos. Chem. Phys., 8, 6117–6136, https://doi.org/10.5194/acp-8-6117-2008, 2008.

1940   Zheng, B., Chevallier, F., Ciais, P., Yin, Y., Deeter, M., Worden, H., Wang, Y. L., Zhang, Q., and He, K. B.: Rapid decline in carbon monoxide emissions and export from East Asia between years 2005 and 2016, Environ. Res. Lett., 13, 044007, https://doi.org/10.1088/1748-9326/aab2b3, 2018a.

1945   Zheng, B., Tong, D., Li, M., Liu, F., Hong, C., Geng, G., et al.: Trends in China's anthropogenic emissions since 2010 as the consequence of clean air actions. Atmospheric Chemistry and Physics,18, 14,095–14,111. https://doi.org/10.5194/acp-18-14095-2018, 2018b.

Zheng, B., Chevallier, F., Yin, Y., Ciais, P., Fortems-Cheiney, A., Deeter, M. N., Parker, R. J.,
1950   Wang, Y., Worden, H. M., and Zhao, Y.: Global atmospheric carbon monoxide budget 2000–2017 inferred from multi-species atmospheric inversions, Earth Syst. Sci. Data, 11, 1411–1436, https://doi.org/10.5194/essd-11-1411-2019, 2019.

Zhi, G. R., Zhang, Y. Y., Sun, J. Z., Cheng, M. M., Dang, H. Y., Liu, S. J., Yang, J. C., Zhang, Y.
1955   Z., Xue, Z. G., Li, S. Y., and Meng, F.: Village energy survey reveals missing rural raw coal in northern China: Significance in science and policy, Environ. Pollut., 223, 705–712, https://doi.org/10.1016/j.envpol.2017.02.009, 2017.